Multiple adsorption of NO on cobalt-exchanged chabazite, mordenite, and ferrierite zeolites: A periodic density functional theory study

ARTICLE *in* THE JOURNAL OF CHEMICAL PHYSICS · SEPTEMBER 2009

Impact Factor: 2.95 · DOI: 10.1063/1.3182850 · Source: PubMed

6 AUTHORS, INCLUDING:

Ivelina Georgieva
Bulgarian Academy of Sciences
57 PUBLICATIONS **468** CITATIONS
SEE PROFILE

Lubomir Benco
University of Vienna
89 PUBLICATIONS **1,390** CITATIONS
SEE PROFILE

Daniel Tunega
University of Vienna
85 PUBLICATIONS **1,306** CITATIONS
SEE PROFILE

N. Trendafilova
Bulgarian Academy of Sciences
84 PUBLICATIONS **796** CITATIONS
SEE PROFILE

Multiple adsorption of NO on cobalt-exchanged chabazite, mordenite, and ferrierite zeolites: A periodic density functional theory study

Ivelina Georgieva,[1,a)] Lubomir Benco,[2,3] Daniel Tunega,[3,4] Natasha Trendafilova,[1] Jürgen Hafner,[2] and Hans Lischka[5]
[1]*Institute of General and Inorganic Chemistry, Bulgarian Academy of Sciences, 11, Acad. G. Bontchev Str., Sofia 1113, Bulgaria*
[2]*Faculty of Physics and Center for Computational Materials Science, University of Vienna, Sensengasse 8, A-1090 Vienna, Austria*
[3]*Institute of Inorganic Chemistry, Slovak Academy of Sciences, Dúbravska cesta 9, SK-84536 Bratislava, Slovac Republic*
[4]*Institute of Soil Research, University of Natural Resources and Applied Life Sciences, Peter Jordan Strasse 82, A-1190 Vienna, Austria*
[5]*Institute for Theoretical Chemistry, University of Vienna, Währingerstrasse 17, A-1090 Vienna, Austria*

(Received 8 May 2009; accepted 26 June 2009; published online 3 August 2009)

The adsorption of NO on Co(II)-exchanged chabazite (CHA), mordenite (MOR), and ferrierite (FER) has been investigated by periodic density functional theory calculations. The most stable configurations of Co(II) in α and β sites of the zeolites with two framework Al/Si substitutions at short distances and Al–$(Si)_{n>1}$–Al ordering are used for calculating the adsorption energy of NO molecules on Co(II) cations and at Al framework sites. The less stable configurations of α-Co(II)-MOR/FER show larger adsorption energies for one and two NO molecules. The bonding of one, two (and three) NO molecules to α/β-Co(II) sites in CHA/MOR/FER induces a shortening of the N–O bond lengths because electron density is withdrawn from the antibonding orbital of the adsorbed NO molecule. The calculated ν(NO) stretching frequencies of mono- and dinitrosyl complexes at α/β-Co(II)-MOR/FER are in good agreement with the experimental data. NO molecules adsorbed on α-Co(II)-MOR and on α-Co(II)-FER show similar NO stretching frequencies as nitrosyl complexes in Co(II)-MOR/-FER/-ZSM-5. Mononitrosyl complexes of α/β-Co(II)-MOR/FER display ν(NO) frequencies blueshifted relative to the free NO, while in dinitrosyl complexes both the symmetric and asymmetric components are redshifted compared to the mononitrosyl frequency. The analysis of the vibrational spectra suggests that mononitrosyls are formed by adsorption at cation in both α and β sites in MOR, FER, and ZSM-5, while dinitrosyl complexes exist only at α-type Lewis sites. This is important for the understanding of the reduction mechanism of NO to N_2. A larger adsorption capacity of α-Co(II)-FER compared to α-Co(II)-MOR is predicted. © *2009 American Institute of Physics*. [DOI: 10.1063/1.3182850]

I. INTRODUCTION

In the light of limited petroleum reserves and stricter air pollution standards, lean burn diesel engines are attractive since they are more fuel efficient than gasoline engines and consequently emit less carbon oxides. The ecological problem is to decrease the concentration of nitrogen oxides in the exhaust at realistic partial pressures of oxygen, which is possible only via the selective catalytic reduction (SCR) of NO_x. Co-exchanged zeolites are notable for their SCR of NO_x with lighter hydrocarbons as reducing agents in the presence of oxygen and water.[1–3] To maximize the efficiency of NO_x reduction catalyzed by Co-exchanged zeolites, the mechanism of NO_x reduction has been studied intensively from both experimental[4–15] and theoretical points of view.[16–21] Understanding the adsorption of NO on Co-exchanged zeolites is the first step toward an improved understanding of the catalytic activity of these zeolites in SCR of NO_x. IR spectroscopy is a technique widely used to identify the nature of the active sites for nitrogen oxide adsorption. However, there are still some controversial assignments of the observed IR bands to different nitrosyl species. Generally, the bands in the 2000–1800 cm^{-1} range are attributed to the stretching vibrations of NO molecules adsorbed at Co cations in the zeolites. Adsorbed NO in different Co(II)-exchanged zeolites such as mordenite (MOR),[13] ferrierite (FER),[2,10] and ZSM-5 (Refs. 2, 4, 14, and 22) show similar vibrational behavior. However, the observed ν(NO) bands have received different assignments in the literature, based on different experimental techniques, conditions of measurements, and comparison with similar transition metal (TM) zeolite systems[2,4] (and literature cited in Ref. 4). A survey of stretching frequencies of NO adsorbed on Co-exchanged zeolites is collected in Table I.[2,4,10,12–14,22,23] Typical IR bands developed upon multiple adsorption of NO on Co(II)-ZSM-5 are displayed in Fig. 1. The analysis of the experimental IR spectra of Co-ZSM-5 by some authors has led to the suggestion that divalent Co(II) stabilizes dinitrosyl species, whereas trivalent Co(III) cations form only mononitrosyls.[4,12] Other authors

a)Electronic mail: ivelina@svr.igic.bas.bg.

TABLE I. Literature survey of IR frequency regions and assignments of NO stretching vibrations of nitrosyl complexes of Co-zeolites.

Frequencies (cm^{-1})	Assignments	Reference
2130–2140 (one band)	$\nu(NO^+)$	4
1956–1930 (set of bands)	ν(NO) (Co(III)-ZSM-5/-BEA)	4, 12, and 23
	ν(NO) (Co(II)-MOR/-FER/-Y/-ZSM-5)	1, 10, 13, and 22
1900–1877 (set of bands)	$\nu_s(NO)_2$ (Co(II)-MOR/-FER/-Y/-ZSM-5/-BEA)	1, 4, 10, 12, 13, 22, and 23
	$\nu(NO^{\delta+})$ (Co(II)-ZSM-5)	14
1810–1794 (set of bands)	$\nu_{as}(NO)_2$ (Co(II)-MOR/-FER/-ZSM-5)	1, 4, 10, 12, 13, 22, and 23
	$\nu(NO^{\delta-})$ (Co(II)-ZSM-5)	14
1857 (one band)	ν(NO) (Co(II)-ZSM-5)	4

suggested that Co(II) ions located at α sites in FER exhibit a higher preference for the formation of dinitrosyl, while Co(II) ions located at β sites form mainly mononitrosyl complexes.[10] Some studies indicated greater rate of NO diffusion than that of Co mononitrosyl formation and decomposition.[24] Thus, a band related to NO bound to the zeolite framework is also expected, although it is not reported in the assignment of the observed bands. (It should mention that adsorbed NO on H-zeolites is not visible in IR spectra.) The bands observed in the 2130–2140 cm^{-1} region have been attributed to NO^+, NO_2^+, or N_2O species adsorbed on framework oxygen atoms.[4,23,25]

Previous theoretical studies of gas-phase nitrosyls indicated that the nature of the TM-NO interaction could be covalent, dative, and electrostatic (charge-dipole interaction) in dependence on the type, the oxidation state of the TM, and the spin state of the M-NO complex.[26] The nature of the TM-NO bonding determines the magnitude and the direction of the changes in the N–O bond length and hence the stretching ν(NO) modes. Therefore, the geometrical structure and vibrational properties of NO adsorption complexes in metal-exchanged zeolites are specific for the metal, its oxidation state, and its location within the zeolite. The crystal-field effects of the zeolite are known to be important for vibrational frequencies of mono- and dinitrosyl species in TM-exchanged zeolite.[27]

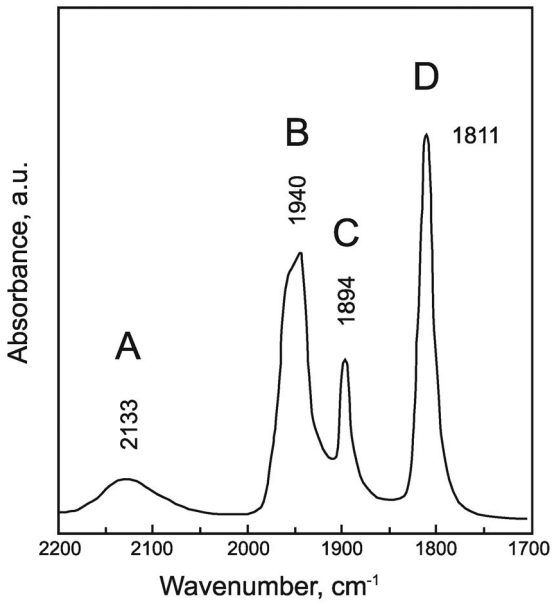

FIG. 1. Sketch of Fourier transform infrared spectra of NO adsorbed on Co-ZSM-5 (according to Ref. 4).

Three different Co(II) positions (α, β, and γ) in MOR, FER, and ZSM-5 were identified on the basis of the characteristic UV/VIS and extended x-ray absorption fine structure spectra and the IR spectra of the skeletal (T-O) vibrations.[6–8] The experimental study of the population of α- and β sites (γ sites play a minor role) in dependence on the Co/Al ratio suggested that (1) the β site is most frequently populated over the whole concentration range; (2) with increasing Co(II) concentration β-population is decreased and α-population increased; (3) under severe thermal/hydrothermal treatment Co(II) moves from the α site to the β site. At the same time, with increasing Co(II) concentration in ZSM-5 and FER, the rate of conversion of NO to N_2 increases. IR spectroscopy of the stretching frequencies of $(NO)_x$ in Co-exchanged zeolites could be successfully applied to study the nature and the type of the active Co ions as well as their adsorption capacity. A reliable interpretation of the IR data, however, requires model calculations of the vibrational properties of adsorbed NO molecules on various Co sites in zeolites. There are different propositions in the literature concerning the possible role of the Co-nitrosyls in the SCR reaction mechanism. The experimental results[4] give no evidence for the formation of $(NO)_2$ dimers in the gas phase and they are not considered in the present theoretical study. Dinitrosyl dimer complexes in the M-zeolites are investigated as hypothetical intermediates of NO decomposition reactions.[28]

Previous experimental investigations of Co-MFI (Ref. 15) and of Co-ZSM-5 (Ref. 29) (using electron paramagnetic resonance and x-ray photoelectron spectroscopy) have shown that the oxidation state of the Co(II) cations was not altered upon oxidation with oxygen, reduction with hydrogen treatment, and interaction with NO at 450 °C. Therefore, in the present work the calculations of Co-exchanged zeolites are performed for Co(II).

Several theoretical studies using cluster models and density functional theory (DFT) have explored the location of the Co cations in FER,[20] ZSM-5,[17] and in zeolite A,[19] and the

energetics and the vibrational modes of adsorbed NO.[20] The calculations have shown the important role of the location of the charge-compensating Al atoms on the framework for the stability of Co(II) sites in the zeolite. In particular, cluster calculations have been used to explore the influence of the choice of the exchange-correlation functional on the adsorption properties because at the moment calculations using hybrid functionals (mixing Hartree–Fock and density functional exchange) are computational rather cumbersome for extended systems. Nachtigall *et al.* studied NO adsorption on Cu(I)-exchanged zeolites using the combined quantum-mechanical/interatomic potential approach[30] and combining DFT calculations on extended systems with cluster calculations.[28] In both cases, hybrid functionals have been used for the cluster calculations. The analysis of these results has shown that hybrid functionals lead to lower adsorption energies, but that the deformation energies (which are determined by the level of theory used for the description of the surrounding) also influence the result.

The aim of the present study is to use periodic density functional calculations to achieve deeper insight into the nature of the active cobalt sites and their ability to adsorb NO molecules. We analyze the relative stabilities of different Co(II) positions for different locations of two framework Al atoms in chabazite, mordenite, and ferrierite and characterize the local geometry of the Co(II) environment. The most probable Co(II) site for NO adsorptions will be chosen on the basis of the calculated adsorption energies of one and more NO molecules. Linear, bent, and side-on structures and spin states of the nitrosyl complexes are examined. The comparison of the calculated stretching frequencies of the adsorbed NO probe molecules with the experimental IR data will help to clarify the type of nitrosyl complexes existing in Co-exchanged zeolites. Our theoretical results are compared with other theoretical studies of TM-exchanged zeolites using periodic and cluster approaches. The possible transferability of the theoretical results for the $(NO)_x$–Co-MOR/FER systems to $(NO)_x$–Co-ZSM-5 is considered and discussed.

II. COMPUTATIONAL DETAILS

A. Structures

The calculations on chabazite are performed for space group $R\bar{3}m$ with the lattice parameters, $a=b=c=9.306$ Å and $\alpha=\beta=\gamma=93.92°$, optimized for the purely siliceous structure.[31,32] The mordenite framework is constructed using the monoclinic primitive cell with optimized parameters, $a=b=13.688$ Å, $c=7.528$ Å, $\gamma=82°$ ($\alpha=\beta=90°$).[33–35] The optimization of the cell parameters of purely siliceous zeolites provides values similar to those experimentally determined on hydrated cation-exchanged structures. The unit cell parameters of ferrierite are taken from the structure determination of K-exchanged dehydrated FER as reported by Cheetham *et al.* ($a=18.651$ Å, $b=14.173$ Å, and $c=7.404$ Å, space group symmetry *Immm*).[36] CHA contains 36 atoms (12 tetrahedral *T* sites and 24 *O* sites) per unit cell, MOR 72 (24 *T* and 48 *O* sites), and FER 108 (36 *T* and 72 *O* sites), respectively. Two aluminum atoms per primitive unit cell were substituted for Si in the CHA, MOR, and FER frameworks, leading to Si/Al ratios of 5 for CHA, 11 for MOR, and 17 for FER, as typical for high-Al zeolites. The two Al/Si substitutions are compensated by the insertion of the divalent Co(II) cation into the unit cell. During the geometry optimization all atoms are free to move, but the lattice vectors of the unit cell and volume are fixed.

B. Exchange-correlation functional

The periodic DFT calculations were performed using the Vienna *Ab initio* simulation package (VASP).[37–40] A crucial point in all DFT calculations is the choice of an exchange-correlation functional. In the present work the exchange-correlation functional proposed by Perdew and Zunger,[41] as corrected for nonlocality in the generalized gradient approximation (GGA) by Perdew and Wang (PW91) (Ref. 42) has been used. For the investigation of molecular adsorption in zeolites the choice is essentially between a conventional semilocal GGA functional (such as PW91) and a hybrid functional mixing exact (Hartree–Fock) and DFT exchange. For molecules and insulating or semiconducting solids, it is now well established that hybrid functionals lead to an improved description of their structural and electronic properties and, in particular, to more realistic predictions for the highest occupied molecular orbital–lowest unoccupied molecular orbital (HOMO-LUMO) energy gap.[43,44] On the other hand it has been found that hybrid functionals fail for metals, in particular, for metals with open *d*-shells. Both in magnetic bulk metals and for magnetic TM atoms and ions the exchange splitting is strongly overestimated.[45,46] Both features are important for the choice of the best functional for studying NO adsorption in Co-exchanged zeolites. Investigations of TM (Fe, Co, and Ni) nitrosyls in the gas phase[47] have shown that for mononitrosyls both GGA and hybrid functionals lead to results of the same overall quality: Hybrid functionals lead to lower and, hence more realistic metal-NO binding energies, but too high NO stretching frequencies. GGA functionals tend to overestimate the binding energies, but produce significantly more accurate vibrational frequencies. For dinitrosyls, however, the binding is correctly described only using GGA functionals. Very recently, similar results have been reported for metal-exchanged zeolites and related materials.[28] It has been shown that at the B3LYP level of theory dinitrosyl complexes are either unstable or only marginally stable in Cu(I) exchanged zeolites. GGA calculations predict stable dinitrosyl complexes with vibrational frequencies in good agreement with infrared spectroscopy. An extended investigation of the relative performance of GGA and hybrid functionals for describing NO adsorption in Cu- and Co-exchanged SAPO-34 (with a CHA-type structure) has recently been presented by Uzunova *et al.*[48] For NO adsorption at Cu(I) cations the adsorption energy is reduced from about 130 to 83 kJ/mol if the GGA functional is replaced by a hybrid functional, in very good agreement with the results reported by Pulido and Nachtigall.[28] For the NO stretching frequencies, the agreement with experiment is much better with the GGA. For divalent cations, however, the differences are much more dramatic: For Cu(II) the cal-

culated adsorption energies are ~85 kJ/mol (GGA) and only ~15 kJ/mol (hybrid functional), for Co(II) the results are ~185 kJ/mol (GGA) and ~65 kJ/mol (hybrid functional). The error in the NO stretching frequencies is less than 10 cm^{-1} (GGA) and about 150 cm^{-1} (hybrid functional). The difference in the performance of both functionals is clearly related to the open *d*-shell of the divalent cation: The increased exchange splitting caused by the admixture of Hartree–Fock exchange shifts the *d*-states of the cations away from the Fermi edge and strongly reduces their interaction with the NO-$2\pi^*$ states. In summary: These results demonstrate that for the investigation of NO molecules at open-shell cations in zeolite GGA functionals lead to a more accurate description than hybrid functionals, although it should not be forgotten that the strength of the adsorbate-cation binding might be overestimated. It should also be pointed out that the NO molecule is a bit a special case: Because of the partial occupation of the $2\pi^*$ state it is pinned at the Fermi level, hence the underestimation of the HOMO-LUMO gap in the GGA is less relevant. The situation might change for the adsorption of CO where the $2p^*$ state is empty and the correct value of the HOMO-LUMO gap is more relevant for the molecule-cation interaction. Investigations of CO adsorption in metal-exchanged zeolites using GGA and hybrid functionals are in progress by Göltl and Hafner.

C. Solving the Kohn–Sham equations, structural optimization

The Kohn–Sham equations were solved variationally with a plane-wave (PW) basis set using an energy cutoff of 400 eV in the projector-augmented-wave (PAW) method of Blöchl[49] as adapted by Kresse and Joubert.[50] Basis-set convergence was tested by performing calculations with a cutoff of 700 eV for isolated NO molecules and neutral and charged Co-nitrosyls. Geometry relaxations were performed using a conjugate-gradient algorithm. Spin polarized calculations were performed with a high accuracy to determine the spin multiplicity in the electronic ground state. The electron configuration d^7 of the Co(II) cation forms either high-spin (HS) configuration with three unpaired electrons and spin multiplicity (SM) equal to 4, or low-spin configuration with one unpaired electron and multiplicity equal to 2. The one unpaired electron in the NO molecule occupies the antibonding orbital (π^*) forming a doublet electronic ground state. In the Co(II)–NO species the spin of the TM cation combines with the unpaired electron of the NO molecule. Depending on the strength of the ligand field three different spin states, quintet, triplet, and/or singlet, can be formed. Brillouin-zone sampling was restricted to the Γ-point. Such a restriction has produced reliable results not only for the medium sized cell of MOR (Ref. 35) and the large unit cell of FER[51,52] but also for the small unit cell of CHA.[31]

The adsorption energy ΔE_{ads} of NO on Co(II)-exchanged zeolites was calculated according to following reaction scheme:

$$(\mathrm{Co-Z})_{opt} + \mathrm{NO} \rightarrow (\mathrm{NO-Co-Z}), \quad (1)$$

where $(\mathrm{Co-Z})_{opt}$ is the optimized structure of the Co-exchanged zeolite (CHA, MOR, FER), the gas-phase NO molecule is optimized in the empty unit cell of the corresponding zeolite, and NO–Co–Z is the optimized configuration of the adsorption complex in the Co-exchanged zeolite. The adsorption energy can be decomposed into two terms,

$$\Delta E_{ads} = \Delta E_{bind} + \Delta E_{strain}. \quad (2)$$

The binding energy ΔE_{bind} includes only the formation of the NO–Co bond and does not account for the deformation energy of the Co(II)-Z structure due to NO adsorption. ΔE_{bind} is computed from single point calculations according to the reaction

$$(\mathrm{Co-Z})_{sp} + \mathrm{NO}_{sp} \rightarrow (\mathrm{NO-Co-Z}), \quad (3)$$

where $(\mathrm{Co-Z})_{sp}$ stands for the Co-exchanged zeolite as distorted upon NO adsorption. The strain energy (ΔE_{strain}) accounts for the Co–Z distortion upon the NO adsorption and it is calculated following the equation:

$$\Delta E_{strain} = E(\mathrm{Co-Z})_{sp} - E(\mathrm{Co-Z})_{opt}. \quad (4)$$

The NO stretching modes of the $\mathrm{Co-(NO)}_x$ complexes were calculated using a finite differences method.[53] Typically, the active part of the structure included approximately ten atoms—the $\mathrm{Co-(NO)}_x$ fragment and several atoms of the surrounding framework. The remaining atoms of the zeolite framework were kept frozen. The reliability of periodic PW91 calculations with PW basis set was checked by PW91 calculations using 6-31+G(*d*), 6-311+G(*d*), and cc-pVTZ Gaussian atomic basis sets[54] for the NO molecule. The calculations were performed using GAUSSIAN 03 program package.[55]

III. RESULTS AND DISCUSSION

A. Test of DFT/LDA-GGA/PW91 method

The reliability of the DFT/PW91 method for calculations of the N–O bond length, stretching mode, and dipole moment was tested in relation to the experimental values. The NO bond length in gas phase,[56,57] ν(NO) vibration in the gas phase,[56–58] and in ZSM-5,[59] and the NO dipole moment in gas phase[60] are collected in Table II. The PW91 calculations performed with a PW cutoff of 400 eV and the smaller local 6-31+G(*d*) basis set give almost identical N–O bond lengths and NO frequencies differing by only ~2 cm^{-1}. The larger local basis set, 6-311+G(*d*), in combination with the PW91 method produces a shorter N–O bond length (by ~0.01 Å) while the stretching frequency remains unchanged. Calculation with a cc-pVTZ basis yields the same bond length and a stretching frequency reduced by 5 cm^{-1}. A larger PW cutoff of 700 eV yields the same bond length and the NO stretching frequency increased by 4 cm^{-1}. We conclude that the calculations with both basis sets are in good agreement and that a PW cutoff of 400 eV is an acceptable compromise between numerical accuracy and the complexity of the NO/cation/zeolite adsorption complexes. The frequencies determined by the force-constant approach are harmonic frequencies, for a comparison with experiments, anharmonic corrections have to be applied. For an isolated molecule the anharmonic frequency shift can be calculated via a numerical solution of the one-dimensional equation of motion for the N–O bond. The

TABLE II. Properties of NO and $[CoNO]^{x+}$ species calculated with different methods and compared to the experimental data.

Species	Method	R(N-O)(Å)	ν(NO) [a](cm^{-1})	μ (D)	SM[b]
NO (isol)[c]	PW91/PAW(400 eV)	1.169	1899	···	2
NO (isol)[c]	PW91/PAW(700 eV)	1.169	1903	···	2
NO (CHA)[d]	PW91/PAW(400 eV)	1.167	1891		
NO (MOR)[d]	PW91/PAW(400 eV)	1.169	1901	···	2
NO	PW91/6-31+G(*d*)	1.168	1897	0.171	2
NO	PW91/6-311+G(*d*)	1.159	1897	0.179	2
NO	PW91/cc-pVTZ	1.158	1892	0.178	2
NO	Experiment	1.158[e]1.154[f]	1876[e,f] (gas) 1872[g] (Ar matrix) 1891[h] (in ZSM-5)	0.153[i]	2
CoNO	PW91/PAW(700 eV)	1.179	1814	···	1
CoNO	BP86/6-311+G(*d*) [j]	1.169	1832	···	1
CoNO	Experiment[j]		1794		
$[CoNO]^+$	PW91/PAW(700 eV)	1.135	2021	···	2
$[CoNO]^+$	BP86/6-311+G(*d*) [j]	1.140	2010	···	2
$[CoNO]^+$	Experiment[j]		1958		
$[CoNO]^{2+}$	PW91/PAW(700 eV)	1.098	2175	···	3
$[CoNO]^{2+}$	PW91/6-311+G(*d*)	1.098	2166	···	3

[a]Calculated harmonic frequencies are unscaled.
[b]Spin multiplicity.
[c]Isolated NO in the unit cell of CHA.
[d]NO located in the cavity of the zeolite (no adsorption).
[e]Reference 56.
[f]Reference 57.
[g]Reference 58.
[h]Reference 59.
[i]Reference 60.
[j]Reference 47.

result is $\Delta\nu_{anharm}=-27$ cm^{-1}, in good agreement with the value of -28 cm^{-1} reported in the literature.[51,52,61] After applying this correction, the agreement between theory and experiment is excellent.

For a NO molecule placed into the center of the large cavities of purely siliceous CHA and MOR (and hence without direct interaction with the framework) only slight changes in the bond length and stretching frequency are calculated. Long-range polarization effect leads to a very small redshift in CHA ($\Delta\nu=-8$ cm^{-1}) and almost no change ($\Delta\nu=2$ cm^{-1}) in MOR, probably due to smaller cavity in CHA. The almost unchanged ν(NO) frequencies for both zeolites (1891 and 1901 cm^{-1}) can be compared to the experimental value for ZSM-5 (1891 cm^{-1}, i.e., blueshifted compared to the gas-phase by ($\Delta\nu=15$ cm^{-1}).[59] The absence of a similar blueshift in the calculations has to be attributed to the neglect of weak long-range correlation in the DFT calculations. The expectation value $\langle S^2\rangle$ of 0.7632 (GAUSSIAN) and magnetic moment of 1 (VASP) calculated for NO molecule suggest doublet spin multiplicity of NO.

A very important characteristic for the charge-dipole interaction of NO with TM is the dipole moment. The PW91 dipole moment well reproduces the experimental one, which is a prerequisite for a reliable calculation of the N–O bond length and frequency changes upon interaction with the metal.

To create a reference for the stretching frequencies of NO adsorbed in the Co-exchanged zeolites, calculations for isolated, neutral and positively charged Co-nitrosyls have been performed. The calculations for the charged species have been performed using periodic boundary conditions, placing the nitrosyl into the center of a large cubic box with an edge measuring 8 Å and applying dipole corrections to compensate for the spurious electrostatic field created by the boundary conditions. The NO stretching frequencies of nitrosyls with a charge of 0 or +1 can be compared with the experimental infrared absorption spectra (IRAS) measured by Zhou and Andrews[47] for matrix-isolated nitrosyls (see Table II, the experimental frequencies listed there are measured in a Ne matrix) and with the DFT calculations performed by these authors using GAUSSIAN and a local 6-311+G(*d*) basis set. These calculations use a slightly different GGA functional (PB86). For both charged and neutral species the ground state has a linear geometry, the spin multiplicities are 1 and 2 for a neutral and a charged nitrosyl. For neutral CoNO electron transfer from the *d*-states of the cation to the antibonding $2\pi^*$ HOMO of the molecule leads to a stretching of the N–O bond length and a redshift of the vibrational frequency [$\Delta\nu=-89$ cm^{-1} (theory) and -82 cm^{-1} (experiment)]. For a positive charge of +1 of the nitrosyl, electrons are withdrawn from the antibonding molecular eigenstate, leading to a contraction of the molecular bond length and a blueshift of the stretching frequency [$\Delta\nu=118$ cm^{-1} (theory) and 82 cm^{-1} (experiment)]. Calculations using PW and local basis sets are in good agreement, considering small differences arising from the choice of the functional. For the charged nitrosyls agreement between theory and experiment is not as good as for the neutral species. It has to be emphasized that in these cases the experimental estimates are derived from peaks with very low intensities. To explore the trend, we have also performed calculations using both local and PW basis sets for a nitrosyl carrying two positive charges, corresponding to the nominal charge of the cation in a Co(II)-exchanged zeolite. In $[CoNO]^{2+}$ the NO bond length is strongly contracted, the NO stretching mode is blueshifted by about 270 cm^{-1}. The re-

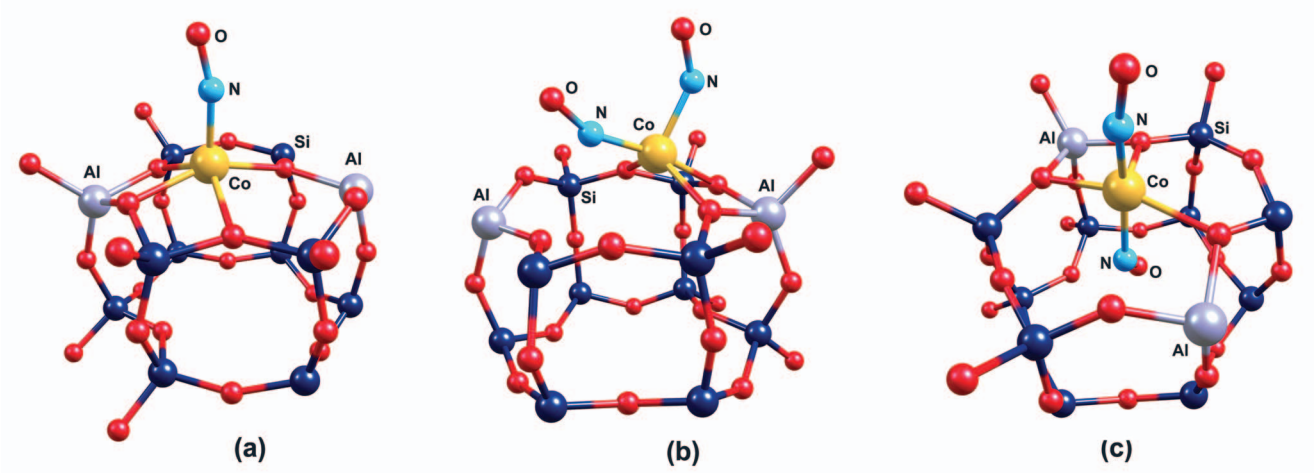

FIG. 2. Mononitrosyl (NO–Co(II)-CHA) (a) and dinitrosyl complexes [*cis*-$(NO)_2$–Co(II)-CHA (b) and *trans*-$(NO)_2$–Co(II)-CHA (c)] formed by adsorption of NO molecules at a Co(II) cation located in a six-membered ring of chabazite.

sults obtained with both basis sets are in excellent agreement. No corresponding mode was found in the IRAS spectra of matrix-isolated nitrosyls. For a comparison of the results obtained using GGA and hybrid functionals, we refer to the work of Zhou and Andrews[47] and of Uzunova *et al.*[48]

B. Stability of Co(II) in CHA: NO adsorption

Chabazite ($Si_{12}O_{24}$) is the simplest zeolite containing three different sites in which Co(II) might be located: four-, six-, and eight-membered rings. The metal location in Zn(II)-CHA and Ca(II)-CHA has previously been studied theoretically.[32,62] The stability of a cationic position depends on the distribution of the two Al atoms. The most stable location was found in the six-membered ring with two Al atoms at opposite sites of the ring (Fig. 2). This metal position is identified with the β site. This is the only configuration of Co(II)-CHA investigated further. Both HS (SM=4, three unpaired electrons) and low-spin (SM=2, one unpaired electron) states of Co(II) (d^7) are investigated in the CHA ligand field. The HS solution for Co(II)-CHA is lower in energy by 30.6 kJ/mol compared to the LS state (Table III). Electron spin resonance experiments for Co(II)-MFI also find a HS state of the Co(II) ions.[15] Also our calculations for Co(II)-MOR and Co(II)-FER find a HS ground state with a magnetic moment of $3\mu_B$ as in the isolated divalent cation. This shows that the ligand field of the zeolite is weak.

The optimized structure of Co(II)-CHA shows four bonds between Co(II) and framework oxygen atoms and a strong framework distortion. The O atoms linked to Al atoms form shorter Co–O bonds, i.e., such O atoms have higher donor abilities.

The adsorption of NO to Co(II)-CHA can occur either through the N- or the O-atom. Comparison of ON-Co(II)-CHA and NO-Co(II)-CHA complexes shows a relative stabilization of the first one by 111 kJ/mol, and a N–Co bond length shorter by 0.12 Å than the O–Co bond, see Table III.

TABLE III. Calculated relative total (ΔE_r, kJ/mol) and adsorption energies (ΔE_{ads}, kJ/mol), selected geometrical parameters (bond length R in Å; angle A in deg) and ν(NO) frequencies (in cm^{-1}) of adsorbed NO on β-Co(II)-CHA. For the dinitrosyl species frequencies for symmetric (s) and asymmetric (as) eigenmodes are listed.

System	SM	ΔE_r	$-\Delta E_{ads}$	R(Co–O) [a]	R(Co–N)	R(N–O)	A(Co–N–O)	ν(NO)
NO[b]	2					1.169		1899
Co(II)-CHA	2	30.6		1.994, 2.040 1.959, 1.901				
Co(II)-CHA	4	0.0		2.133, 2.051 2.012, 1.993				
NO–Co(II)-CHA (via N atom)	5	122.6	166.1	2.252, 2.129 2.029, 2.016	1.867	1.177	171	···
NO–Co(II)-CHA (via N atom)	3	0.0	184.7	2.191, 2.099 2.150, 2.016	1.688	1.158	164	1938
NO–Co(II)-CHA (via N atom)	1	18.6	62.1	2.082, 2.064 1.975, 1.964	1.743	1.172	131	···
NO–Co(II)-CHA (via O atom)	3	111.1	73.6	2.106, 2.161 2.110, 2.023	1.805[a]	1.169	169	···
cis-$(NO)_2$–Co(II)-CHA	2	0.0	98.9[sec] 283.6[tot]	2.187, 2.092 2.037	1.776 1.700	1.163 1.153	135 157	1943_s 1838_{as}
trans-$(NO)_2$–Co(II)-CHA	2	48.6	50.4[sec] 235.1[tot]	2.100, 2.084 2.038	1.851 1.705	1.159 1.155	136 170	1950_s 1851_{as}

[a]Distances between Co and O in CHA.
[b]Isolated NO in the unit cell of CHA.

The adsorption energies for the N/O adducts are 185/74 kJ/mol. Hence, the molecule-cation bonding via the O atom is more than two times weaker. Similar differences in N/O bonding are observed for NO adsorption on Fe(II)-exchanged ferrierite.[51] For this reason it is expected that NO adsorption on Co(II) cations in zeolites takes place only through the N atom. In the remainder of our paper the notation NO-Co(II) will be used for the N-bonded adsorption complex.

The optimization of the NO–Co(II)-CHA complex was performed with the three possible input geometries: linear, bent, and side-on. The calculations have been performed in a fixed-moment mode with spin of $S=2$, 1, and 0 for the NO-Co(II) complex. An isolated NO–Co(II) nitrosyl (see Table II) has a linear geometry, the neutral nitrosyl has a $S=0$ ground state while the negatively and positively charged nitrosyls have $S=1/2$.

The optimized NO–Co(II)-CHA configuration is presented in Fig. 2(a). The calculations predict a triplet spin ground state followed by the closed shell (singlet) and the HS state (quintet), see Table III. Therefore, upon adsorption of NO, a pairing of the NO $1\pi^* \uparrow$ electron with a Co $d_\sigma \downarrow$ electron occurs, leading to triplet spin state and a magnetic moment of $2\mu_B$. The same ground state was found for the NO–Co(II) cluster in all intrazeolite configurations studied. In line with the increasing stability of NO–Co(II)-CHA in the spin states quintet, singlet, and triplet, the adsorption energy of NO increases, and the Co(II)–N and N–O bond lengths decrease. However, in the ground state the N–O bond length and the N–O stretching frequency are intermediate between the values calculated for a neutral and a positively charged gas-phase nitrosyl. This suggests that due to the interaction with the charged zeolite framework with two Al substitutions, the effective charge on the Co cation is reduced to a value slightly below +1.

Upon NO adsorption the Co(II)–O(CHA) bond lengths in the open-shell triplet and quintet states are elongated, whereas in the closed-shell singlet state they are shortened. Parallel to the decreasing Co–O(CHA) bond lengths in the ^5A, ^3A, ^1A states, the Co–N–O angle also decreases from 171° (^5A) to 164° (^3A) and 131° (^1A). It is worth noting that in the triplet state of the NO–Co(II)-CHA complex the N–O bond length is shorter, whereas in the quintet and singlet states the N–O bond lengths are slightly longer than in the gas phase. The NO molecule in the NO–Co(II)-CHA (^3A) complex shows a blueshifted ν(NO) frequency (at 1938 cm^{-1}) compared to the values calculated for a gas-phase NO (1899 cm^{-1}) or an unbound NO in the center of the CHA cavity (1891 cm^{-1}), see Table III.

The formation of a dinitrosyl species on the β-Co(II) cation in CHA is favored. Table III lists the total adsorption energy and the differential adsorption energy for the second NO molecule. Relative to the plane formed by the four Co–O bonds, the two NO molecules can adsorb to Co(II) in *cis* or in *trans* positions, cf. Figs. 2(b) and 2(c). The larger adsorption energy of the second NO in a *cis*-position shows that this configuration is preferred by 48.6 kJ/mol. The shorter Co–N bond lengths in the *cis*-complex are accompanied by longer Co–O bond lengths. Obviously the *cis*-$(NO)_2$ configuration allows a larger distortion of the CHA framework causing a weaker Co–O bonding. Following the bond-order conservation rule the adsorption of the second NO molecule leads to a disruption of one of the Co–O bonds, only three bonds of Co to O atoms neighboring to Al atoms in the six-membered ring are conserved. The adsorption of two NO molecules in a *cis*-position leads to blueshifted symmetrical (at 1943 cm^{-1}) and redshifted asymmetrical (at 1838 cm^{-1}) stretching frequencies compared to the free ν(NO) frequency (at 1899 cm^{-1}), see Table III. The calculations reveal the following vibrational properties of mono- and dinitrosyls formed at the β site of Co(II)-CHA: (1) *cis* and *trans* $(NO)_2$ adsorptions produce similar vibrational behavior and (2) the ν(NO) frequency of a mononitrosyl species (1938 cm^{-1}) approaches the symmetrical ν(NO) frequency (1943 cm^{-1}) of adsorbed dinitrosyl species.

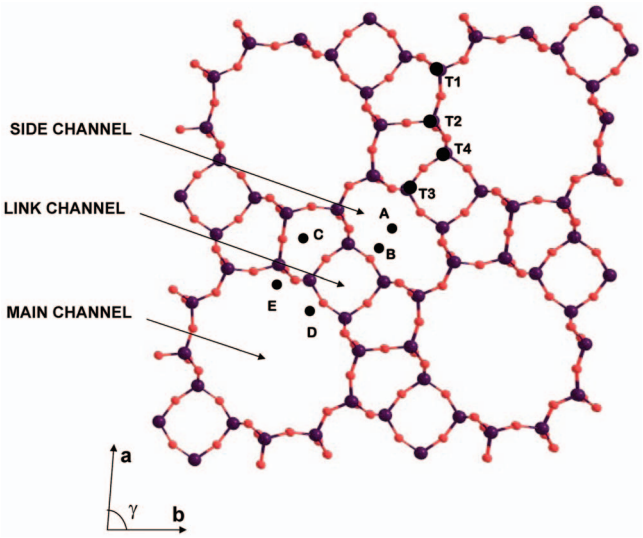

FIG. 3. Structure of mordenite (MOR) viewed along the *c*-axis showing different channels within the framework. T1, T2, T3, and T4 are the four inequivalent types of framework tetrahedral sites. A (β site), B, C, D, and E (α site) show the extraframework positions as classified by Mortier (Ref. 63).

C. Energetics and vibrational properties of $(NO)_x$–Co(II)-MOR

1. Stability of Co(II) in mordenite

The structure of mordenite consists of a main channel composed of 12-membered rings, 8-membered oval-shaped side channels, and a link channel, see Fig. 3. Possible locations of extraframework cations have been classified by Mortier.[6,9,63] The analysis of the experimental data suggests that Co(II) in MOR occupies mainly Mortier sites *E* (β-positions) and *A* (α-positions), see Fig. 3. Our calculations for Co(II) in MOR are performed for (1) the α-position in the *E* site in the six-membered ring of the main channel and (2) the β-position in the *A* site, located in the oval-shaped eight-membered ring of the side channel.

As already discussed, the locations of the two Al/Si substitutions in the framework are important for the stability of the cation location in a metal-exchanged zeolite.[33–35] Experimental techniques have not been able to determine the ar-

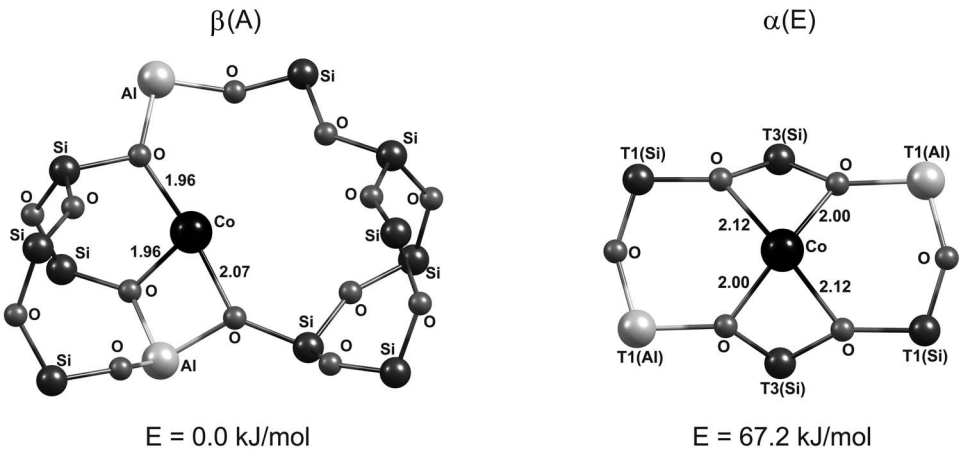

FIG. 4. The most stable configurations of a Co(II) cation located at Mortier positions A and E of MOR and their total energies relative to the most favorable configuration with Co(II) in site A. The $\alpha(E)$ configuration with two Al/Si substitutions of Co(II) in T1 sites. The bond lengths are given in Å.

rangement of Al atoms around the cation sites. Detailed theoretical studies of the Al distribution in Zn-MOR and Pd-MOR have been performed by Benco *et al.*[35] and Grybos *et al.*[64] using periodic DFT calculations. In the present work the stability of Co(II) locations in MOR is investigated for $Al-(O-Si)_2-O-Al$ sequences obeying Loewenstein's rule[65] supported by NMR data.[66,67] As stated in the literature, configurations with two Al atoms at short distances dominate in a zeolite with a low Si/Al ratio (<6), i.e., in high-Al zeolites. Configurations with the extraframework cation close to two Al sites are more stable than those with the cation near just one Al site.[51]

Seven possible positions of the two charge-compensating Al atoms were considered for a Co(II) cation in eight-membered ring of MOR (β-position). Figure 4 shows the location of the two Al atoms in the most stable β- and α-Co(II)-MOR structures. All other Al–Al arrangements produce higher energy structures. Since the β-Co(II) complex is more stable than all α-Co(II)-MOR structures, its energy is taken as a reference. Binding of the Co(II) cation in a β-position in MOR is achieved through three bonds to O atoms in the ring, connected to the Al atoms. The predicted most stable β-Co(II)-MOR configuration is consistent with the experimental finding that predominantly β sites are occupied at all Co loadings in Co(II)-MOR.[6] The calculated Co–O bond lengths of 1.96–2.07 Å agree well with the experimental values, 1.99–2.06 Å deduced from VIS experiments.[9] The same stable location in the β-position of MOR was also reported for other divalent cations (Ca(II), Cu(II), Pd(II)).[64,68]

According to the total energy calculations, the most stable location of Co(II) at α-positions in MOR (E site) is realized with two Al atoms occupying opposite corners of the six-membered ring in T1 sites, see Fig. 4. α-Co(II) is coordinated to four framework oxygen atoms, two of them are neighbors to Al atoms. α-Co(II) with two Al atoms in T3 sites is lower in energy than the configuration displayed in Fig. 4. However, the two Al atoms in T3 sites are connected by a short Al–O–Si–O–Al sequence bridging the ring (see the discussion in Ref. 34). Such a configuration with two Al atoms in T3 sites of the same ring is not observed in NMR experiments.[66,67] This configuration is therefore not considered as an active site for adsorption of NO.

In addition, another α-Co(II) position in the D site (Fig. 3) was calculated with Co(II) coordinated to two O atoms with short Co(II)–O distances (~1.91 Å). However, the calculated $\alpha(D)$-Co(II) structure is less stable (by ~9 kJ/mol) compared to $\alpha(E)$-Co(II)-MOR. The $\alpha(E)$-Co(II)-MOR complex is higher in energy by 67 kJ/mol compared to the most stable β-Co(II)-MOR structure, therefore the α site will be occupied only at high Co loadings. This finding is supported by experiments revealing that the α-Co(II) occupation increases with increasing Co loading.[6,9] In the following, NO adsorption is studied for the two stable β-Co(II)-MOR and α-Co(II)-MOR configurations shown in Fig. 4.

2. NO adsorption on β- and α-Co(II)-MOR

Figure 5 shows the correlation between the adsorption energy of NO and the total energy of the Co(II)-MOR configurations. Geometric parameters and NO adsorption energies of $(NO)_x-Co(II)$-MOR complexes are compiled in Table IV. To simulate multiple NO adsorption by successive addition of small NO doses, differential adsorption energies for up to three NO molecules per Co(II) cation at β-Co(II)-MOR or α-Co(II)-MOR sites and on Al sites of the framework have been calculated. A schematic sketch of the

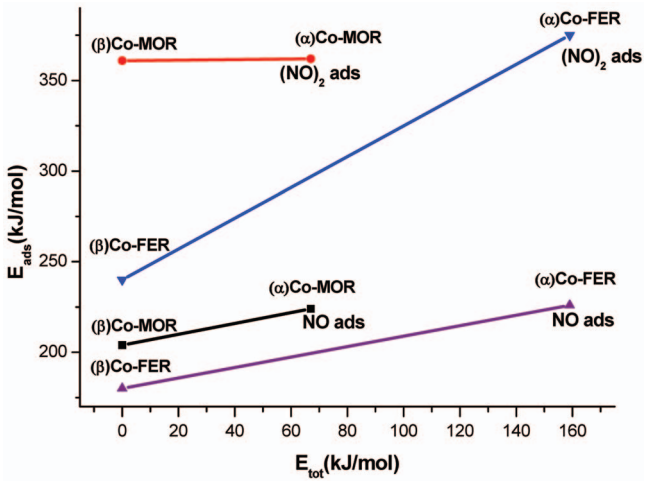

FIG. 5. Adsorption energies E_{ads} of one and two NO molecules on Co(II) cations in β and α sites of MOR and FER, plotted vs the relative total energies E_{tot} of the β- and α-Co(II) configurations.

TABLE IV. Adsorption energies (ΔE_{ads}, in kJ/mol) and selected geometrical data (bond length R in Å, angle $\angle$ in deg) of $(NO)_x$–Co(II)-MOR (x=1, 2, 3).

System	$-\Delta E_{ads}$	R(Co–O)	R(Co–N)	R(O···N)	R(N–O)	$\angle$ (Co–N–O)	$\angle$ (N–Co–N)	$\angle$ (O–Co–O)
NO[a]					1.169			
NO–α-Co(II)-MOR	224.0	2.033, 2.187 2.044, 2.181	1.681		1.153	178		134 (145)[b]
NO–β-Co(II)-MOR	204.1	2.218, 2.026 1.940	1.691		1.152	158		149
cis-$(NO)_2$–α-Co(II)-MOR	362.1	2.046, 2.346	1.717		1.152	154	106	122
	(224.0+138.1) [c]	2.066	1.742		1.161	139		
trans-$(NO)_2$–β-Co(II)-MOR	361.5	2.118, 2.028	1.727		1.149	161	128	
	(204.1+157.4) [c]	2.253	1.699		1.148	155		
cis-$(NO)_2$–β-Co(II)-MOR	243.5	2.195,1.959	1.908		1.159	128	90	
	(204.1+39.4) [c]		1.681		1.149	156		
cis-$(NO)_2$–α-Co(II)-MOR-NO	452.0	2.215, 2.091	1.661	2.15	1.162, 1.167	152	101	106
	(362.4+89.9) [c]		1.666	3.33	1.128[d]	156		
cis-$(NO)_2$–β-Co(II)-MOR-NO	424.6	2.031, 2.122	1.650	1.95	1.163,1.167	158	106	
	(361.5+63.1) [c]		1.649	3.05	1.127[d]	161		
NO^+				2.050	1.126			
(ads in MOR)				2.237				

[a]Isolated NO in the unit cell of MOR.
[b]$\angle$(O–Co–O) in α-Co(II)-MOR.
[c]Adsorption energy of the precursor plus differential adsorption energy of the last added NO.
[d]NO adsorbed on the MOR framework.

adsorption geometry, together with differential and integral adsorption energies is given for β- and α-configurations in Figs. 6 and 7, respectively. Adsorption of one NO on Co(II) is exothermic and the adsorption energies are 204 kJ/mol for β(A)-Co(II)-MOR and 224 kJ/mol for α(E)-Co(II)-MOR. Low adsorption energy of only ~40 kJ/mol is calculated for NO molecules bound to Al atoms of the MOR framework. Hence at low loading NO adsorbs only on the Co(II) cation and not on Al sites. As seen from Fig. 5, with the decreasing stability of the cation location in the order β-Co(II)-MOR $>\alpha(E)$-Co(II)-MOR, the adsorption energy per NO molecule increases. To evaluate the relative importance of the coordinative unsaturation of the cation and of the strain on the framework, the adsorption energy is decomposed into (1) the binding energy ΔE_{bind} used as indicator of the intrinsic Co(II)–NO bond strength and (2) the strain energy related to the deformation of the surroundings of the cation. The calculated binding energies of NO with α-Co(II)-MOR (235 kJ/mol) and β-Co(II)-MOR (219 kJ/mol) indicate that adsorption is intrinsically favored by ~16 kJ/mol on the α site. The adsorption-induced strain energy is found to be quite modest, for α-Co(II)-MOR (11 kJ/mol) it is by 4 kJ/mol smaller than that for β-Co(II)-MOR (15 kJ/mol). Therefore, the larger ΔE_{bind} and the smaller ΔE_{strain} of NO–α-Co(II)-MOR are responsible for the stronger NO adsorption on α-Co(II) and the ΔE_{bind} (related to the coordinative unsaturation of Co) is the dominant contribution to the adsorption energy.

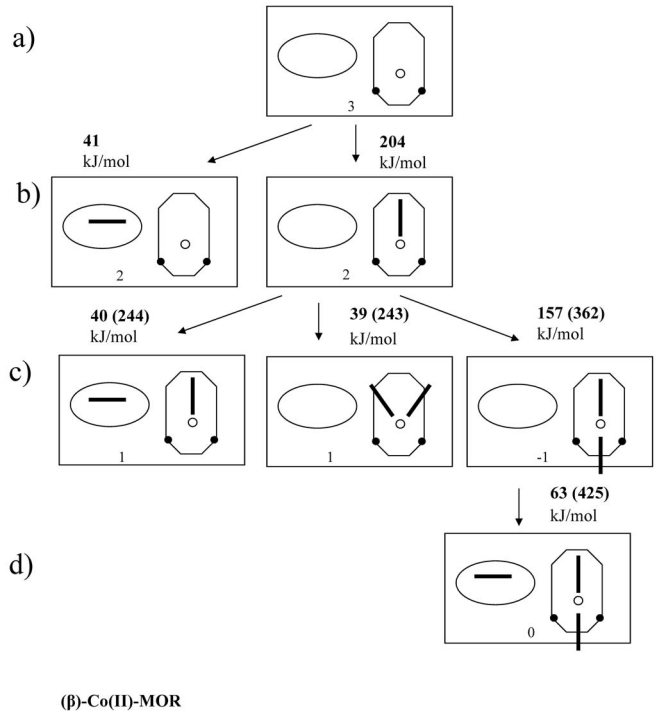

FIG. 6. Schematic geometry and adsorption energies of up to three NO molecules adsorbed to Co(II)-MOR with Co(II) in the β site. Ovals/octagons represent main/side channels of the framework. Circles and full dots stand for Co(II) cations and framework Al atoms. Sticks represent NO molecules. (a) shows the configuration without NO, [(b)–(d)] the configurations with one to three adsorbed NO molecules. The arrow indicates the addition of one NO, the numbers next to the arrows the differential adsorption energies in kJ/mol and the total adsorption energies (in parentheses). The magnetic moments in μ_B (bottom of the panel) are listed for each configuration.

Generally, the adsorption of NO on Co(II)-MOR leads to shorter N–O bond lengths (by 0.016 and 0.017 Å), see Table IV, and blueshifted stretching NO frequencies (by 54–69 cm^{-1}) compared to free NO, see Table V. The reduction in the NO bond length and the blueshift of the stretching mode are smaller than for $[CoNO]^+$ (ΔR=−0.034 Å, $\Delta\nu$ =122 cm^{-1}) and much smaller than for $[CoNO]^{2+}$ (ΔR= −0.071 Å, $\Delta\nu$=276 cm^{-1}). Infrared spectroscopy on matrix-isolated charged $[CoNO]^{x+}$ also shows a roughly linear variation of the NO stretching frequency with the charge state of the cation. Hence we agree with the suggestion of Zhou and Andrews[47] that the effective charge state of the Co cation in

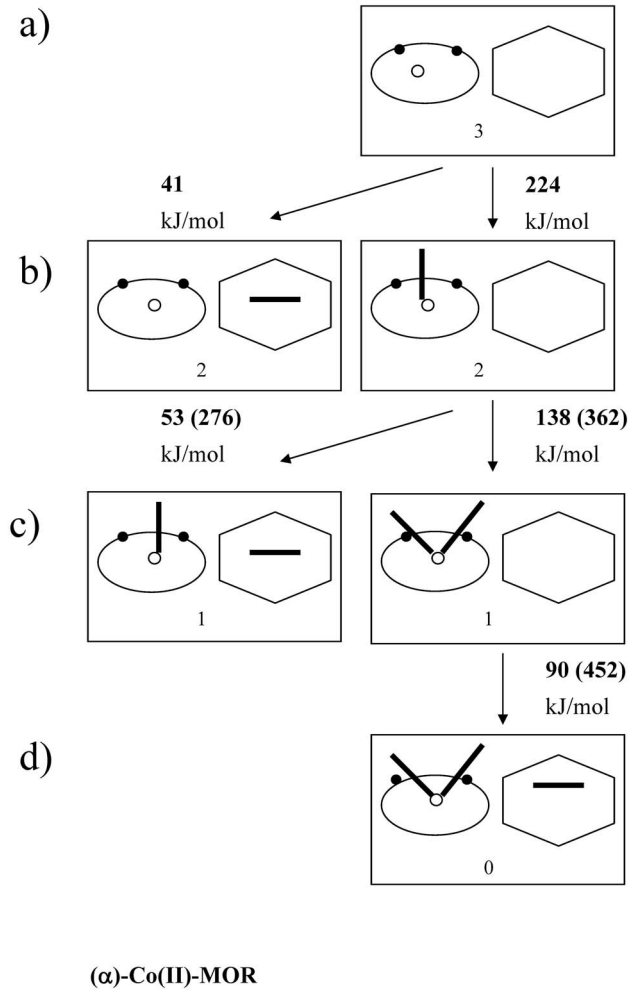

FIG. 7. Adsorption configurations and adsorption energies of up to three NO molecules on Co(II)-MOR with Co(II) in the α site. Cf. Fig. 6.

Co(II)-MOR is definitely lower than +1 due to charge-compensation between the cation and the Al sites on the framework. Similar to NO–Co(II)-CHA, the Co–N-O complex in NO–Co(II)-MOR has a bent geometry. The factors responsible for the change from a linear (in the isolated $[CoNO]^+$ and CoNO nitrosyls) to a bent geometry in NO–Co(II)-MOR are related to the geometry of the Co(II)-MOR complex and to a rehybridization of the *d*-states of the cation due to the binding to the framework. The linear geometry of the isolated nitrosyls arises from the formation of π-bonds between the π^* states of the molecule and $d\pi$ states of the metal. The nearly square-pyramidal bonding geometry of Co(II) in the six-membered ring shows that mostly Co t_{2g} orbitals build the Co–O bonds between the cation and the framework. Due to the participation of the d_π (t_{2g}) states in the Co–O bonds, charge is transferred mostly to d_σ-states and bond formation between these states and the molecular π^* state is possible only in bent adsorption geometry. The interaction between $2\pi^*$ orbital of adsorbed NO and d_π orbital of Co for NO–α(Co)-MOR complex is visualized in Fig. 8(a). The arrows show electron density transfer from NO $2\pi^*$ to Co d_π.

The stronger interaction of NO with $\alpha(E)$-Co(II)-MOR compared to β-Co(II)-MOR correlates with the corresponding Co–N bond lengths, 1.681 and 1.691 Å, respectively, while the N–O bond lengths are similar, 1.153 and 1.152 Å. The Co–N–O angle shows a large flexibility in dependence on the Co(II) position: NO–$\alpha(E)$-Co(II)-MOR forms a nearly linear geometry (178°), whereas in NO–β-Co(II)-MOR, the Co–N–O angle is smaller by ~20°. Formation of configurations with different Co–N–O angles leads to bonding mechanisms which break the correlation between the Co–N and N–O bond lengths.

The exothermic adsorption energies of a second NO molecule on α- and β-Co(II) indicate that the adsorption of two NO molecules on Co-exchanged MOR is favored, see Table IV and Figs. 6 and 7. Upon adsorption of a second NO molecule, spin pairing of the electron in the singly occupied $2\pi^*$ state with a Co *d*-electron reduces the spin of the $(NO)_2$–Co(II)-MOR complex to $S=1/2$, the ground state is a doublet. All possible adsorption sites of the second NO molecule were investigated: On an oxygen atom of the MOR framework, on α-Co(II) and β-Co(II) cations in both *cis* and *trans* configurations, see Figs. 6 and 7. It should be mentioned that a *trans*-$(NO)_2$ configuration on the α-Co(II) site is not possible due to steric hindrance. The strongest adsorption of a second NO was found for the β-Co(II) site in a *trans* position ($\angle$(N–Co–N)=128°), see Table IV and Fig. 6. The *cis*-$(NO)_2$–β-Co(II)-MOR structure ($\angle$(N–Co–N) =90°) is higher in energy by 118.1 kJ/mol. On the α-Co(II)-MOR site, adsorption in a *cis* configuration leads to almost the same adsorption energy as for a *trans*-dinitrosyl on β-Co(II).

The adsorption of two NO molecules leads to an elongation of the Co–O distances and reduces the number of Co(II)–O bonds to 3. The dinitrosyl complexes have bent geometries ($\angle$(Co–N–O) ~ 140–160°) and the adsorbed NO molecules show shorter bond lengths compared to the free NO molecule, compared to the mononitrosyls they remain about the same.

When we attempt to optimize the structure of a $(NO)_3$–α-Co(II)-MOR trinitrosyl complex one NO molecule moves away and binds to a framework oxygen close to an Al atom. This means that a $(NO)_2$–Co(II)-MOR complex has no adsorption capacity to form a cluster with three NO molecules directly coordinated the Co(II) cation. The adsorption of a third NO molecule on the framework, however, increases the bond strength between the Co(II) cation and the NO molecules in the dinitrosyl because the number of Co–O bonds is reduced to 2, increasing the coordinative unsaturation of the Co(II) cation. Nonetheless, the tendency toward spin pairing between the added NO molecule and the Co(II)-MOR complex continues, after adsorption of a third NO molecule the ground state is a singlet. The total adsorption energy of three NO molecules is larger for $(NO)_2$–α-Co(II)-MOR–NO compared to $(NO)_2$–β-Co(II)-MOR–NO due to the larger adsorption energy of the first NO on the Co(II) cation and the third NO on the Al site of the MOR framework, see Figs. 6 and 7.

3. NO stretching frequencies

The NO stretching frequencies ν(NO) calculated for $(NO)_x$ adsorption complexes on Co(II) in α- and β-positions

TABLE V. Calculated harmonic NO stretching frequencies (in cm^{-1}) for nitrosyl complexes of β-/α-Co(II)-MOR/FER. Comparison with available experimental values.

		MOR		FER	
Configuration/site	CHA	β	α	β	α
NO[a]	1899	1901		1902	
NO^+ (ads)			2045		
Mononitrosyl	1938	1955	1970	1959	1976
cis-dinitrosyl	1943_s	1975_s	1939_s		1948_s
	1838_{as}	1835_{as}	1855_{as}		1881_{as}
cis-dinitrosyl+NO		2025	2028		2050
		1926_s	909_s		1907_s
		1876_{as}	1850_{as}		1856_{as}
trans-dinitrosyl	1950_s	1998_s		1895_s	
	1851_{as}	1944_{as}		1801_{as}	
trans-dinitrosyl+NO				1966	
				1825_s	
				1750_{as}	
trinitrosyl+NO					2011
					1968
					1823_s
					1778_{as}
$(NO)_x$ in Co-MOR (exp., Ref. 13)		1952, 1940, 1897, 1814			
$(NO)_x$ in Co-FER (exp., Ref. 10)				1935, 1898, 1815	
$(NO)_x$ in Co-ZSM5 (exp., Ref. 4)				2133, 1970, 1957, 1940, 1894, 1811 (1857)	
$(NO)_x$ in Co-H-MFI (exp. Ref. 12)				2137, 1958, 1945, 1901, 1817(1854, 1758)	

[a]Isolated NO in the unit cell of CHA/MOR/FER.

of MOR are compiled in Table V. As discussed above, the adsorption of one NO molecule leads to a shortening of the N–O bond length in relation to the free NO molecule and hence to a blueshifted ν(NO) stretching frequencies. The stronger interaction of NO with α-Co(II) produces a larger blueshift of ν(NO) to ~1970 cm^{-1} compared to the β site [ν(NO)=1955 cm^{-1}].

In dinitrosyl complexes of Co(II)-MOR, the N–O bond lengths are also shorter than in free NO. *Trans*-$(NO)_2$–β-Co(II)-MOR cluster represents a relatively symmetric configuration with similar N–O bond lengths and ∠(Co–N–O) angles for both molecules, whereas in *cis*-$(NO)_2$–α-Co(II)-MOR and *cis*-$(NO)_2$–β-Co(II)-MOR clusters N–O bond lengths and ∠(Co–N–O) angles differ by up to 0.01 Å and 28°, respectively. *Trans*-$(NO)_2$ adsorption on β-Co(II) leads to blueshifted symmetric (~90 cm^{-1}) and asymmetric (~40 cm^{-1}) ν(NO) vibrations, see Table V. *Cis*-$(NO)_2$ adsorption on α-Co(II) and β-Co(II), however, gives a blueshifted (75–40 cm^{-1}) symmetric ν(NO) bands and redshifted (65–45 cm^{-1}) asymmetric ν(NO) bands, reflecting the large differences in the two N–O bond lengths (see Table IV).

The adsorbed third NO molecule in the eight-membered ring of the MOR framework and in the main channel of MOR exhibits a NO stretching frequency strongly blueshifted to 2025 and 2028 cm^{-1} with respect to the free NO, respectively. The large blueshift correlates with strongly contracted N–O bond lengths. The frequencies are similar to the value of ~2100 cm^{-1} which is attributed to the stretching frequency of NO^+ adsorbed at a cation position in zeolite[25] but lower than the frequency of ~2200 cm^{-1} assigned to an isolated NO^+ ion.[69] To distinguish the $\nu(NO^+)$ and ν(NO) modes, we performed calculations of NO^+-exchanged MOR. For a NO^+ cation in a hypothetical NO^+-exchanged structure, where the NO^+ cation compensates one Al/Si framework substitution, the calculated $\nu(NO^+)$ frequency is 2045 cm^{-1}, similar to the values obtained for the third NO molecule adsorbed to the framework close to the cation Co(II) (Table V). Note that adsorption of a third NO molecule on the zeolite framework induces a pronounced rearrangement of the bonding within the $(NO)_2$–Co adsorption complex, leading to changes of N–O bond lengths and ν(NO) stretching fre-

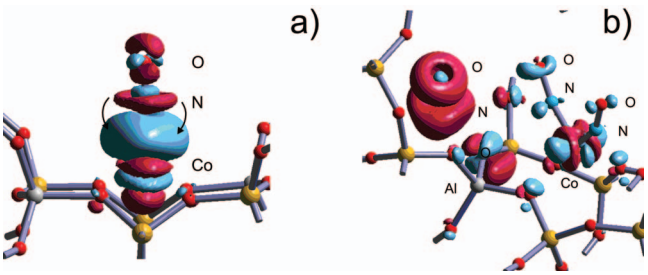

FIG. 8. Flow of the electron density induced by adsorption of the NO molecule at bare Co^{2+} cation (a) and dinitrosyl $Co^{2+}(NO)_2$. Blue (light gray) regions indicate a gain and the red (dark) regions a depletion of the electron density (same isosurfaces apply for both figures).

quencies. The N–O bond lengths are elongated and the ν(NO) frequencies of the symmetric modes are lowered. Both phenomena, the pronounced shortening of the bond length of the third NO molecule adsorbed on the Al site and the elongation of the bond lengths in the dinitrosyl, can formally be described in terms of a redox reaction,

$$[Co(NO)_2]^{2+} + NO \leftrightarrow [Co(NO)_2]^{+} + NO^{+}. \quad (5)$$

The antibonding $2\pi^*$ state of the NO molecule bound to the framework is depleted as shown in Fig. 8(b). The huge depletion of π-density on NO is due to oxidation of the third molecule to NO^+. This explains the strong contraction of its bond length and the blueshifted NO stretching mode. The framework oxygen atom neighboring to NO^+ is strongly polarized. Increased density on two NOs indicated reduction to NO^-. The transferred charge [Eq. (5)] locally compensates the charge deficit around the Al atom on the framework so that the compensation of the charge of the Co(II) cation is reduced. This results in a weaker bonding between the cation and the framework and a stronger Co(II)–NO bond (see Table IV) while N–O bond lengths are slightly stretched (backdonation from Co to π^* NO states). The charge state assigned in Eq. (5) to the dinitrosyl and the NO bound to the framework should not be identified with static electric charges. The change in the charge states of the $Co(II)-(NO)_2$ and the Al–O–NO complexes also results in a rehybridization of all bonds such that changes in the local charges remain small—we refer to the recent discussion of the correlation between formal oxidation states and static electric charges of TM ions in semiconductors and insulators by Raebiger *et al.*[70] Similar changes in the formal charge state of the TM nitrosyl were recently observed also at high loading of NO in Fe^{2+}-exchanged zeolite.[52,63] The reaction is induced by a local compensation of the positive framework charges by the electron transfer from the neutral NO molecule, leading to a reduced charge compensation on the TM cation—which is in turn counterbalanced by the rehybridization of the $Co(II)-(NO)_2$ complex.

In conclusion, for low NO loading, the adsorption occurs first on the α-Co(II)-MOR site, followed by adsorption on β-Co(II)-MOR with ν(NO) frequencies blueshifted to 1970 and 1955 cm^{-1}. Hence, the bands observed at 1952 and 1940 cm^{-1} could be attributed to mononitrosyls in Co(II)-MOR (Ref. 13) (in a comparison between theory and experiment, one has to remember that the calculated harmonic frequencies have to be corrected by $\Delta\nu \sim -27$ cm^{-1} for anharmonicity). With increased NO loading, dinitrosyl complexes are formed on the α-Co(II)-MOR with a blueshifted symmetric ν(NO) mode at 1939 cm^{-1} and a redshifted asymmetric ν(NO) mode at 1855 cm^{-1}. Further increase in NO loading leads to the adsorption of NO molecules on framework oxygen atoms connected to Al sites of the MOR framework, formally resulting in an extraframework NO^+ cation whose stretching frequency correlates with the IR band observed at ~2100 cm^{-1}. The two components of the dinitrosyl, which are lowered by the coadsorption (see Table V), could, after correction for anhamonicity, be assigned to bands observed at 1897 and 1814 cm^{-1}.[13]

D. Energetics and vibrational study of $(NO)_x$–Co(II)-FER

1. Stability of Co(II) in ferrierite

In order to estimate the role of the zeolite type, the adsorption capacity and bonding properties of a Co(II) cation are further studied in FER. The α and β sites are the most probable positions for an extraframework Co(II) cation, as experimentally suggested from the VIS spectral components of Co(II) ions in FER, see Fig. 9.[7,8] The α-Co(II) cation occupies the center of a six-membered ring in the wall of the main channel. The β-Co(II) cation is located in a distorted six-membered ring of the FER side channel. Experimental data predict that the α- and β-locations of the Co(II) cation, and the Co–O bond lengths are the same for FER and ZSM-5. Therefore, it is expected that the theoretical results obtained for Co(II)-FER are valid also for Co(II)-ZSM-5. In line with the experiments predicting the highest population of Co(II) in the β-position over a broad concentration interval of Co(II) in FER, the Co(II) location in the β site (Al atoms in T4 sites) forms the most stable configuration, see Fig. 10(a).[7] The calculated Co–O bond lengths in β-Co(II)-FER are 1.98–1.99 Å, in excellent agreement with experiment.[9,10] For the Co(II) cation in the β site two different distributions of the Al atoms in the framework are possible: Two Al in T4 sites or in T2 sites forming a *trans*-configuration. Because the latter configuration is considerably less stable (ΔE=+111 kJ/mol), we study NO adsorption only for the former configuration with Al atoms in T4 sites [Fig. 10(a)]. In the α site [Fig. 10(b)] two Al atoms in T3 sites form the most stable configuration. However, Al atoms in the two T3 sites are connected by a Al–O–Si–O–Al sequence on the back side of the ring, which is excluded by NMR experiments. For studying the adsorption of NO in Co(II)-FER, we use the configuration with two Al atoms in T1 sites [Fig. 10(b)] which is by ~160 kJ/mol less stable than the β-Co(II) site [Fig. 10(a)].

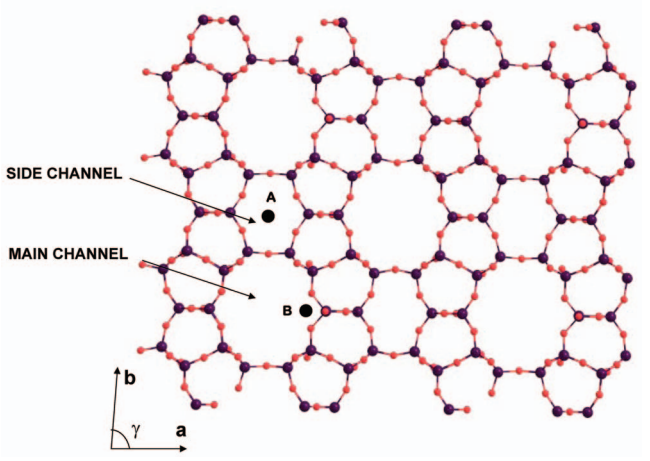

FIG. 9. The structure of ferrierite (FER) viewed along the *c*-axis. The most populated positions of extraframework cations are marked A (β site) and B (α site); site B is located at the wall of the main channel (MC) and site A in a six-membered ring of the side channel (SC).

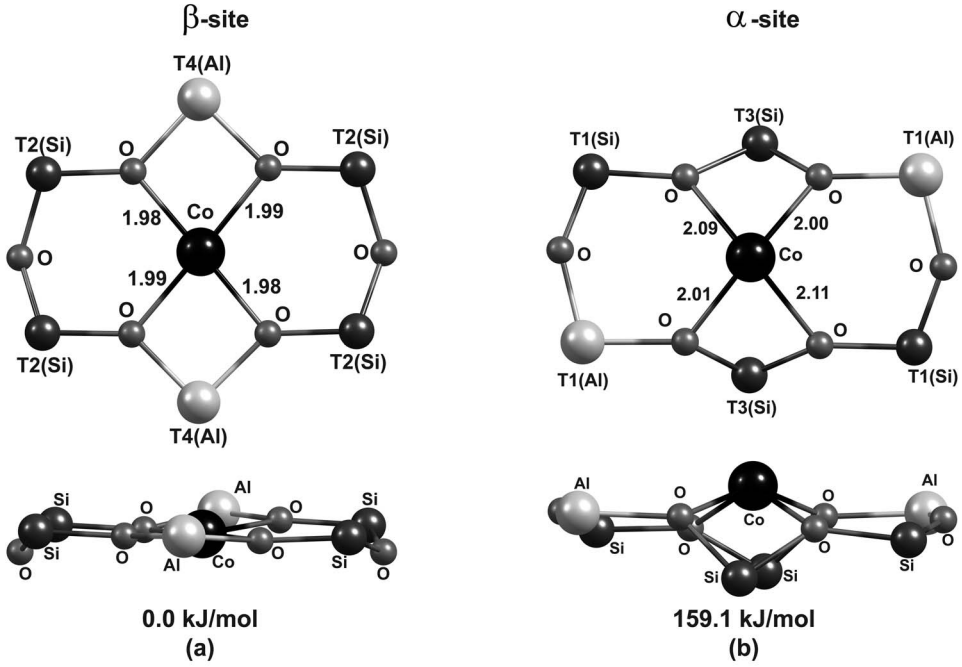

FIG. 10. The two most stable configurations of a Co(II) cation in ferrierite. (a) Geometry of the β-Co(II)-FER site with two Al/Si substitutions in T4 sites. (b) Configuration of the α-Co(II)-FER site with two Al/Si substitutions in T1 sites. Distances between the Co(II) and framework oxygen atoms are given in Å; total energies are given relative to the most stable β-Co(II)-FER site.

2. NO adsorption on β and α sites in Co(II)-exchanged FER

The capacity of Co(II)-FER to adsorb one or many NO molecules in α and β sites (Fig. 9) was studied and compared with adsorption on Fe(II)-FER.[51,52] Adsorption energies and geometrical parameters of the Co-exchanged FER and $(NO)_x$–Co(II)-FER clusters are collected in Table VI. The calculated stretching frequencies of NO adsorbed on Co(II)-FER are given in Table V.

Differential adsorption energies of NO molecules adsorbed on Co(II) in the α and β sites and on the Al site in the Co(II)-FER are displayed in Figs. 11 and 12, respectively. For a single NO molecule, the calculated adsorption energy is 29/52 kJ/mol on the Al site [Figs. 11(b) and 12(b), left] and 180 and 226 kJ/mol on the Co cation for β/α-Co(II) configurations [Figs. 11(b) and 12(b), right]. The large difference indicates that at low loading, NO adsorbs almost exclusively on the Co(II) cation. The larger adsorption energy of the less stable α-Co(II) configuration shows that in spite of higher concentration of Co(II) in β sites, at low loading the most favorable center for adsorption is α-Co(II). The same trend was observed for a different zeolite [α- and β-Co(II)-MOR, see above] and also for a different TM cation [α- and β-Fe(II)-FER].[52] Previous computational studies based on a cluster approach have also predicted a higher NO adsorption energy on α-Co(II) than on β-Co(II) in FER.[21]

TABLE VI. Calculated adsorption energies (ΔE_{ads}, in kJ/mol) and selected geometrical data (bond length R in Å; angle ∠ in deg) of $(NO)_x$–Co(II)-FER (x=1–4).

System	$-\Delta E_{ads}$ [a]	R(Co–O)	R(Co–N)	R(N–O)	∠(Co–N–O)	∠(N–Co–N)	∠(O-Co-O)
NO[b]				1.169			
NO–α-Co(II)-FER	225.5	2.136, 2.054 2.060, 2.156	1.680	1.154	179		137
NO–β-Co(II)-FER	179.8	2.062, 2.049 2.054, 2.054	1.682	1.156	172		146
cis-$(NO)_2$–α-Co(II)-FER	375.0	1.993, 2.039	1.703	1.159	157	104	121
	(149.5+225.5)		1.734	1.153	144		
trans-$(NO)_2$–β-Co(II)-FER	239.6	2.049, 2.163	1.867	1.159	136	172	177
	(59.8+179.8)	2.072, 2.104	1.775	1.161	129		
$(NO)_3$–α-Co(II)-FER	443.4	2.167, 2.016	1.689, 1.695	1.151, 1.151	158, 156	91, 108	109
	(68.4+375.0)		2.116	1.154	123	89	
cis-$(NO)_2$–α-Co(II)-FER-NO	464.0	2.063, 2.284	1.656, 1.658	1.165, 1.168	158	106	104
	(89.0+375.0)			1.125[c]	155		
trans-$(NO)_2$–β-Co(II)-FER-NO	277.6	2.085, 2.167	1.793	1.168	134	173	179
	(38.0+239.6)	2.060, 2.143	1.841	1.169	131		
				1.144[c]			
				1.153, 1.173		105	80
$(NO)_3$–α-Co(II)-FER-NO	560.6	2.017	1.658, 1.772	1.169	175, 142	112	
	(96.6+464.0)		1.756	1,126[c]	142	109	

[a]Values in parentheses give the decomposition of the adsorption energy into that of the precursor plus the differential adsorption energy of the last added NO.
[b]Isolated NO in the unit cell of FER.
[c]NO adsorbed on the FER framework.

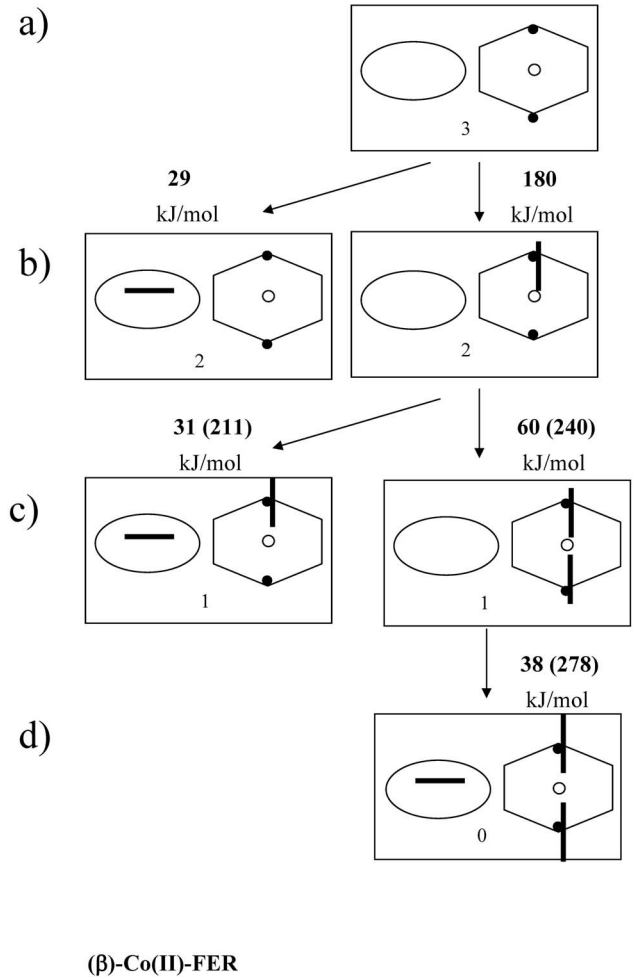

FIG. 11. Schematic representation of the adsorption configurations and adsorption energies of up to three NO molecules on Co(II)-FER with Co(II) in the β site. Cf. Fig. 6.

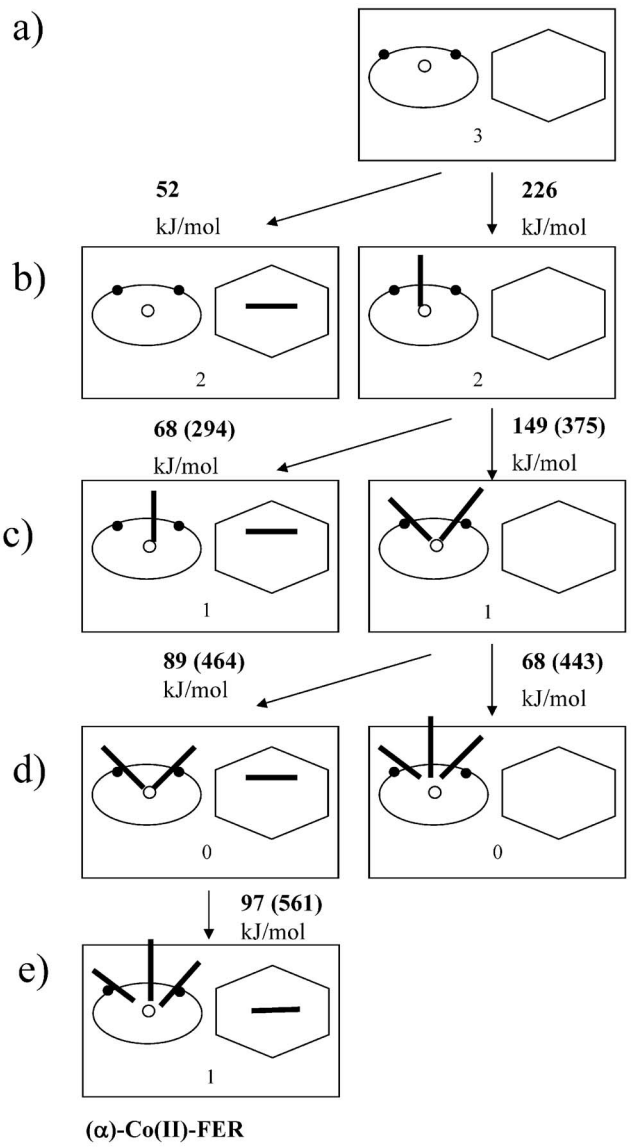

FIG. 12. Schematic representation of the adsorption configurations and adsorption energies of up to four NO molecules on Co(II)-FER with Co(II) in the α site. Cf. Fig. 6.

However, the calculated adsorption energies of NO on Co(II)-FER from our periodic approach are larger by 40–70 kJ/mol (absolute value) than those obtained using cluster models [DFT/BP86 method and LANL2DZ basis set for Co(II)], revealing the effect of the zeolite framework. Two energy components mainly contributing to the ΔE_{ads} of NO are (1) the binding energy, $\Delta E_{\text{bind}}=-234.9/-221.0$ kJ/mol (α/β-Co(II)), and (2) the strain energy, $\Delta E_{\text{strain}}=9.4/41.1$ kJ/mol (α/β-Co(II)). Therefore, larger NO adsorption energy on α-Co(II) of 226 kJ/mol compared with 180 kJ/mol on the β-Co(II) site is due to stronger intrinsic bonding and a considerably lower strain. Similar values for the binding energies indicate that the coordinative unsaturation of both sites is similar. The observed difference in the adsorption energies of 46 kJ/mol thus originates mainly from the different local flexibilities of the adsorption sites.

The adsorbed NO molecule on both Co(II)-FER sites forms nearly linear geometry: The $\angle$Co–N–O angle is 172° for NO–β-Co(II) and 179° for NO–α-Co(II). Parallel to the similar values of the intrinsic NO–Co(II) binding energies on α- and β-Co(II)-FER, the Co–N and N–O bond distances are almost the same (differences are only 0.002 Å). These differences are even smaller than for NO adsorption on α- and β-Co(II)-MOR where the difference in the adsorption energies is lower. This emphasizes again that the different adsorption properties of Co(II) in α and β sites of FER arises from a lower flexibility of the framework surrounding the β site. However, due to the asymmetric position of Co(II) in the β site of MOR, a different bonding between Co(II) and NO leads to a different geometry of the Co–N–O adduct (cf. the Co–N–O angle of 158°).

Comparison of mononitrosyls on Co(II)-CHA/MOR/FER and Fe(II)-FER.[51] The adsorption of one NO molecule on Co(II) in CHA, MOR, and FER produces shorter N–O bond lengths than the gas-phase NO value. A similar shortening of the N–O bond length after adsorption on Fe(II)-FER has been explained by electron density accumulation in the bond between the Fe(II) cation and NO and the proportional depletion of the antibonding $2\pi^*$ state of the NO molecule.[51] Comparison of data on NO–α-Co(II)-MOR (Table IV) and NO–α-Co(II)-FER (Table VI) shows similar NO adsorption

energies, N–Co(II) and N–O bond lengths, and ν(NO) frequencies (Table V), demonstrating the similar adsorption properties of the α-Co(II) site in MOR and FER. On the other hand, comparison of the data for NO–α-Co(II)-FER and NO–α-Fe(II)-FER (Refs. 51 and 52) indicates a lower NO adsorption energy of the Fe(II)-FER site (~5 kJ/mol) and a lower ν(NO) stretching frequency (~40 cm^{-1}), revealing the influence of a lower *d*-band occupancy. The bond length of a NO molecule adsorbed on Fe(II)-FER is slightly longer than in Co(II)-FER. It should be mentioned that the ν(NO) frequency of the NO–Cu(II)-ZSM5 is also blueshifted, whereas for the NO–Cu(I)-ZSM5 complex, it is redshifted.[71] This demonstrates that NO adsorption on Fe(II), Co(II), and Cu(II) cations leads to qualitatively similar results, with quantitative differences arising from the different degrees of *d*-band filling and spin state for the different cations and to some extent also from the properties of the zeolite framework. Cu(I) cations represent a special case because of the closed-shell nature of the isolated cation bonding to the framework and adsorbate bonding require other mechanisms.

For a second NO molecule the preferred adsorption site is the Co(II) cation. On the α-Co(II) a *cis*-, on the β-Co(II) site a *trans*-configuration of the dinitrosyl complex is preferred, the ground state is in any case a doublet, see Figs. 11 and 12. The total adsorption energies of two NO molecules on Co(II)-FER indicate a much higher stability of the *cis*-complex on the α-Co(II)-FER site (ΔE_{ads}=−375 kJ/mol) compared to *trans*-complex on β-Co(II)-FER (ΔE_{ads}=~−240 kJ/mol), see Table VI. Therefore, the less populated α-Co(II)-FER site is found to be more active also for dinitrosyl formation. The adsorbed NO molecules on α-Co(II)-FER have shorter N–O bond lengths than in the gas phase and bent geometries with ∠O–N–Co angles of 157° and 144°. The adsorption of the second NO molecule on the α-Co(II)-FER site leads to a pronounced change of bonding. The Co(II) cation moves above the plane of the six-membered ring and forms a quasitetrahedral coordination with only two strong bonds to framework oxygen atoms, similar to the bonding configuration of the α-Fe(II)-FER dinitrosyl.[52] Dinitrosyl formation on the β-Co(II) site leads to a much more modest change in the Co(II)-framework bonding: All four Co(II)–O bonds are conserved, they are only stretched by 0.013–0.114 Å. Hence the restricted ability for dinitrosyl formation is again a consequence of the low local flexibility of the framework. A much smaller stabilization of the *trans*-dinitrosyl complex at the β-Co(II) site compared to α-Co(II) site is in agreement with previous suggestions that mononitrosyl formation occurs simultaneously on the α- and β-Co(II)-FER sites, whereas the dinitrosyl complex is realized mainly on the α-Co(II)-FER site.[10]

To investigate adsorption at high loading with NO, the binding of three and four NO molecules to Co(II)-FER was also modeled. The ground state of a trinitrosyl complex is a singlet as for MOR, but after adsorption of a fourth NO molecule, no further spin pairing is possible, the ground state is a doublet. Adsorption of three NO molecules on the α site can lead to the formation of a *cis*-trinitrosyl-Co(II)-FER complex [Fig. 12(d), right] or to a dinitrosyl-Co(II)-FER with third NO molecule binding to the framework [Fig. 12(d), left]. In α-Co(II)-FER both configurations coexist, with an energy difference of only 20 kJ/mol (see Table VI)—this implies that the two configurations are separated by a migration barrier for the NO molecule. The formation of a trinitrosyl at α-Co(II)-FER is in contrast to the situation for α-Co(II)-MOR where the third NO molecule migrates to the framework. Close to a trinitrosyl complex in the α-position, even a fourth NO molecule can be adsorbed, binding to a framework oxygen connected to the Al site. The differential heat of adsorption for this fourth molecule at the trinitrosyl complex is even higher than for adsorption at a dinitrosyl.

The adsorption of a third and fourth NO molecule changes the bonding of the Co(II) cation to the framework: the two Co–O bonds remaining after dinitrosyl formation are further elongated, and after adsorption of a fourth molecule only one strong Co-framework bond of 2.02 Å remains. The change in the N–O bonding upon adsorption of two, three, or four NO molecules on α-Co(II)-FER is similar to that observed on Co(II)-dinitrosyls in MOR (cf. above) and on Fe(II)-dinitrosyls in FER.[52] For the di- and trinitrosyl, the N–O bond lengths are only slightly contracted compared to the bond length in a mononitrosyl. Upon adsorption of a NO molecule on a nearby framework site, the N–O bond lengths in the di- or trinitrosyl are elongated, while the bond length of the NO molecule bound to the framework is strongly contracted to about 1.125 Å. As discussed above, we interpret this in terms of the formation of an extraframework NO^+ cation and a concomitant reduction in the positive charge on the $Co(NO)_{2(3)}$ complex.

A *trans*-trinitrosyl is unstable at the β site. This is not surprising since already the second NO in the dinitrosyl is only weakly bound — the situation is similar to the *trans*-β-Fe(II)-FER complex.[52] A third NO molecule can only weakly adsorb to the zeolite framework [Fig. 11(d)] with an energy gain of 38 kJ/mol. Compared to the dinitrosyl complex this leads to an elongation of the N–O bonds by about 0.01 Å, while the NO molecule bound to the framework is contracted to 1.144 Å (i.e., less than for adsorption close to an α site). Hence the reduced flexibility of the framework around the β site also limits the charge rearrangement upon multiple NO adsorption.

3. NO stretching frequencies

Stretching frequencies of $(NO)_x$ complexes formed on Co(II)-exchanged FER are listed in Table V together with those of $(NO)_x$ complexes on Co(II)-MOR. For both zeolites with increasing number of adsorbed NO molecules a similar variation of the frequencies is observed. All mononitrosyls exhibit frequencies in the range of 1950–1980 cm^{-1}, blueshifted with respect to gas-phase ν(NO) of ~1901 cm^{-1}. After an anharmonicity correction of 27 cm^{-1}, calculated for both gas-phase NO and NO adsorbed on Fe(II)-FER,[51] the ν(NO) of mononitrosyls is in good agreement with the main band in the IR spectra of Co(II)-MOR,[13] Co(II)-FER,[10] and Co(II)-ZSM-5 (Ref. 4) centered at 1940 and 1935 cm^{-1}, respectively (band B in Fig. 1). The scatter of the stretching frequencies for α and β sites indicates that the broad band

ranging from 1920 to 1980 cm^{-1} detected in the experiments originates from mononitrosyls formed on different Co(II) adsorption sites.

NO molecule in *trans*-dinitrosyls in MOR and FER show different vibrational behavior. In MOR the symmetric-asymmetric splitting produces two frequencies, one similar to the frequency of the mononitrosyl (1944 cm^{-1}) and one blueshifted to 1998 cm^{-1}. Formation of this configuration therefore leads to a broadening of the main IR band B toward higher frequencies (Fig. 1). Note, however, that because of the off-centered position of the cation in MOR, the geometry of the configuration is far from a true *trans*-configuration (the N–Co–N angle is $\approx 128°$). In FER, where a true *trans*-configuration is formed, both ν(NO) values are redshifted to lower frequencies (1895 and 1801 cm^{-1}). The low adsorption energy indicates, however, that only a minor contribution to bands C and D (Fig. 1) from true *trans*-dinitrosyl can be expected. *Cis*-dinitrosyls on α sites of MOR and FER show a splitting of similar character [$\Delta(\nu_s\text{-}\nu_{as}) \sim 70-80$ cm^{-1}]. Both components are redshifted compared to the mononitrosyl frequency. *Cis*-dinitrosyls thus contribute to bands C and D (Fig. 1). A NO molecule added to a *cis*-dinitrosyl produces a strongly blueshifted mode at 2020–2060 cm^{-1}, slightly lower than the stretching frequency of an isolated NO^+ cation. These frequencies compare well with the broad experimental band A at 2040–2180 cm^{-1} (Fig. 1) assigned to NO^+ cations occupying cationic positions in the zeolite.[4,25] The binding of the two NO molecules to the TM cation is weakened, the stretching frequencies are lowered (Table V), and thus better fit in the range of bands C and D (Fig. 1).[4,10,13] The anharmonicity correction lowering the calculated frequencies by about 27 cm^{-1} additionally improve the result. Experiment has revealed that upon the NO loading at 500 Pa equilibrium pressure the intensity of the band B decreases and the intensities of the bands C and D increase.[4] According to our calculations, the band B was assigned to mononitrosyl complex, whereas the other two bands C and D to dinitrosyl complexes. The decrease in the intensity of band B could be related to lower stability of the mononitrosyl as compared to that of the dinitrosyl species, in agreement with the calculated exothermic dinitrosyl formation (adsorption of the second NO).

Trinitrosyl is formed only at high NO loading in Co(II)-FER. When in addition a NO molecule is bound to the framework [Fig. 12(e)], one ν(NO) mode of the trinitrosyl is similar to the frequency of the mononitrosyl, while two frequencies are lowered to 1823 and 1778 cm^{-1}, respectively (Table V). These lowest frequencies could be assigned to the IR band D (Fig. 1). Bonding within NO adducts on Co(II) thus differs from that on Fe(II), where the lowest ν(NO) frequencies are observed for the dinitrosyl and a third NO molecule bound to the Fe(II) cation causes an increase in the NO stretching frequencies.[52]

IV. CONCLUSIONS

An extensive theoretical study of the adsorption capacity of Co(II) exchanged in different zeolites (CHA, MOR, and FER) for one to four NO molecules has been performed using periodic density functional calculations. Based on total energy calculations for Co(II)-CHA/MOR/FER with two Al/Si substitutions placed at short distances [i.e., in one ring, following the $Al-(Si)_{n>1}-Al$ rule], the most stable configurations of α-Co(II) and β-Co(II) sites in MOR and FER have been selected. In all studied zeolites, Co(II) cation exists in a HS (quartet) state. The calculated higher stability of β-Co(II)-MOR/FER configurations compared to α-Co(II)-MOR/FER correlates with the larger population of the β-Co(II) sites observed in experimental studies at all concentrations of Co(II). Total energy calculations predict that the less stable α-Co(II)-MOR/FER sites exhibit higher NO adsorption energy than the corresponding β-Co(II) sites. A higher intrinsic binding energy related to the coordinative unsaturation of α-Co(II) and a smaller strain energy related to a higher local flexibility of the framework are responsible for the stronger NO adsorption on α-Co(II)-MOR/FER. For the stabilization of NO–α-Co(II)-MOR configurations the coordinative unsaturation of Co(ΔE_{bind}) plays the decisive role, whereas for NO–α-Co(II)-FER a much smaller strain energy is also important.

Bonding of NO on Co(II)-CHA and α/β-Co(II)-MOR/FER induces a pronounced shortening of the NO bond length because electron density is withdrawn from the antibonding $2\pi^*$ orbital of the adsorbed NO molecule. A correlation between the NO adsorption energy and the Co–N and N–O bond lengths is found for NO–Co(II)-FER configuration, but it is less evident for NO–Co(II)-MOR with a strongly bent geometry of the nitrosyl [$\angle$(CoNO) $< 180°$].

The NO stretching frequencies calculated for the stable Co(II)-CHA and α/β-Co(II)-MOR/FER configurations are blueshifted with respect to the free NO molecule and agree well with the experimental bands observed upon NO adsorption on Co(II)-MOR/-FER/ZSM-5.[4,10,12,13] The different values of the stretching frequency calculated for α- and β-mononitrosyls suggest that a broad experimental band ranging from 1920 to 1980 cm^{-1} originates from mononitrosyls formed on different Co(II) adsorption sites. Simulation of the adsorption of two to four NO molecules on α/β-Co(II) sites and on nearby framework sites in MOR and FER shows the preferred formation of *cis*-dinitrosyl complexes on α-Co(II)-MOR/FER and for Co(II)-CHA, and a larger adsorption capacity of α-Co(II)-FER compared to α-Co(II)-MOR and Co(II)-CHA. A third NO molecule adsorbed in the vicinity of a *cis*-Co(II)-MOR/FER dinitrosyl binds to a framework oxygen connected to an Al site and leads to a charge rearrangement formally described as a redox reaction $NO \rightarrow NO^+$ and $[Co(NO)_2]^{2+} \rightarrow [Co(NO)_2]^+$. Both particles together compensate the two Al/Si framework substitutions. The calculated stretching frequencies of the intrazeolite NO^+ cation of $\sim$2030 to 2050 cm^{-1} correlate with an IR band at 2040–2180 cm^{-1}. The scenario is analogous to that recently observed for Fe(II)-FER.[52] The reduction in the charge on the $Co(NO)_x$ complex leads to an elongation of the bond length and to a decrease in the NO stretching frequencies. Both $\nu(NO)_2$ components are redshifted relative to the mononitrosyl frequency, indicating that the bands at

~1898 and ~1815 cm^{-1} originate from dinitrosyls. The change in bonding and the formation of the $[Co(NO)_2]^+$ complex increase the adsorption capacity of the TM cation in FER and enable further adsorption and formation of a trinitrosyl $[Co(NO)_3]^+$ complex.

The present work shows that α-Co(II)-MOR/FER and Co(II)-CHA exhibit a similar geometrical and vibrational properties of adsorbed mono- and dinitrosyls. This explains why the NO stretching frequencies in the extraframework Co–NO cluster is only weakly dependent on the zeolite framework. The long-lived NO^+ cation observed in experimental studies is produced at a locally increased concentration of NO due to the complex reaction which formally includes the change in the charge state of the di- or trinitrosyl complex. The role of the NO^+ cation in activity of the TM-exchanged zeolite, however, is not clear and merits further investigations.

Our investigations are based on periodic models of the zeolite framework and a semilocal GGA exchange-correlation functional, hence they fully account for the deformability of the structure and provide a reliable structure of the adsorbate/cation/zeolite complex. However, while the GGA leads to vibrational frequencies in very good agreement with experiment, it is known to tend to overestimate adsorption energies. This means that trinitrosyl or dinitrosyl+NO configurations, for which GGA calculations have predicted a low exothermic heat of formation (50 kJ/mol or smaller), could eventually be unstable or only marginally stable. In the vibrational spectra, the signature of these configurations is the strongly blueshifted frequencies beyond 2000 cm^{-1}. The comparison with the experimentally detected modes suggests that such configurations could be unstable in MOR and FER, but exist in ZSM5.

ACKNOWLEDGMENTS

The work is supported by Bulgarian Science Fund Grants Nos. DO-02-233 and DO-02–82, by the Austrian Science Fund (FWF) under Project Nos. P20893-N19 and P19983, and by the German Research Foundation (DFG) within the priority program SPP1315, Project No. GE1676/1. I.G. acknowledges financial support by the Austrian Academy of Sciences during her stay at the Institute for Theoretical Chemistry, University of Vienna, in the framework of the Bilateral Exchange Agreement Austria-Bulgaria. The work was partially supported by the Centre of Competence on Multifunctional Materials and New Processes with Environmental Impact (Project MISSION, Contract No. EC-INCO-CT-2005-016414). The calculations were performed in part on the Schrödinger III cluster of the University of Vienna.

[1] Y. Li and J. N. Armor, J. Catal. **150**, 376 (1994).
[2] Y. Li, T. L. Slager, and J. N. Armor, J. Catal. **150**, 388 (1994).
[3] Y. Li and J. N. Armor Appl. Catal., B **5**, L257 (1995); J. N. Armor, Catal. Today **26**, 147 (1995).
[4] K. Hadjiivanov, E. Ivanova, M. Daturi, J. Saussey, and J.-C. Lavalley, Chem. Phys. Lett. **370**, 712 (2003).
[5] K. Hadjiivanov, B. Tsyntarski, and T. Nikolova, Phys. Chem. Chem. Phys. **1**, 4521 (1999).
[6] J. Dědeček and B. Wichterlová, J. Phys. Chem. B **103**, 1462 (1999).
[7] D. Kaucký, J. Dědeček, and B. Wichterlová, Microporous Mesoporous Mater. **31**, 75 (1999).
[8] J. Dědeček, D. Kaucký, and B. Wichterlová, Microporous Mesoporous Mater. **35-6**, 483 (2000).
[9] L. Drozdová, R. Prins, J. Dědeček, Z. Sobalík, and B. Wichterlová, J. Phys. Chem. B **106**, 2240 (2002).
[10] Z. Sobalík, J. Dědeček, D. Kaucký, B. Wichterlová, L. Drozdová, and R. Prins, J. Catal. **194**, 330 (2000).
[11] D. Kaucký, A. Vondorová, J. Dědeček, and B. Wichterlová, J. Catal. **194**, 318 (2000); J. Dědeček, D. Kaucký, and B. Wichterlová, Top. Catal. **18**, 283 (2002).
[12] C. Resini, T. Montanari, L. Nappi, G. Bagnasco, M. Turco, G. Busca, F. Bregani, M. Notaro, and G. Rocchini, J. Catal. **214**, 179 (2003); T. Montanari, O. Marie, M. Daturi, and G. Busca, Catal. Today **110**, 339 (2005).
[13] L. B. Gutierrez, E. E. Miró, and M. A. Ulla, Appl. Catal., A **321**, 7 (2007).
[14] T. Sun, M. D. Fokema, and J. Y. Ying, Catal. Today **33**, 251 (1997).
[15] E. M. El-Malki, D. Werst, P. E. Doan, and W. M. H. Sachter, J. Phys. Chem. B **104**, 5924 (2000).
[16] M. J. Rice, A. K. Chakarborty, and A. T. Bell, J. Phys. Chem. A **102**, 7498 (1998).
[17] M. J. Rice, A. K. Chakraborty, and A. T. Bell, J. Phys. Chem. B **104**, 9987 (2000).
[18] S. A. McMillan, R. Q. Snurr, and L. J. Broadbelt, J. Phys. Chem. B **107**, 13329 (2003).
[19] K. Pierloot, A. Delabie, C. Ribbing, A. A. Verberckmoes, and R. A. Schoonheydt, J. Phys. Chem. B **102**, 10789 (1998).
[20] S. A. McMillan, L. J. Broadbelt, and R. Q. Snurr, J. Phys. Chem. B **106**, 10864 (2002).
[21] S. A. McMillan, L. J. Broadbelt, and R. Q. Snurr, J. Catal. **219**, 117 (2003).
[22] M. C. Campa, S. de Rossi, G. Ferraris, and V. Indovina, Appl. Catal., B **8**, 315 (1996).
[23] F. Geobaldo, B. Onida, P. Rivolo, F. Di Renzo, F. Fajula, and E. Garrone, Catal. Today **70**, 107 (2001).
[24] E. M. Sadovskaya, A. P. Suknev, L. G. Pinaeva, V. B. Goncharov, B. S. Bal'zhinimaev, C. Chupin, and C. Mirodatos, J. Catal. **201**, 159 (2001).
[25] K. Hadjiivanov, J. Saussey, J. L. Freysz, and J.-C. Lavalley, Catal. Lett. **52**, 103 (1998).
[26] J. L. C. Thomas, Ch. W. Bauschlicher, Jr., and M. B. Hall, J. Phys. Chem. A **101**, 8530 (1997).
[27] P. Treesukol, J. Limtrakul, and T. N. Truong, J. Phys. Chem. B **105**, 2421 (2001).
[28] A. Pulido and P. Nachtigall, Phys. Chem. Chem. Phys. **11**, 1447 (2009).
[29] T. Sun, M. L. Trudeau, and J. Y. Ying, J. Phys. Chem. **100**, 13662 (1996).
[30] M. Davidova, D. Nachtigallova, and P. Nachtigall, J. Phys. Chem. B **108**, 13674 (2004).
[31] Y. Jeanvoine, J. Angyan, G. Kresse, and J. Hafner, J. Phys. Chem. B **102**, 5573 (1998).
[32] L. A. M. M. Barbosa, R. A. van Santen, and J. Hafner, J. Am. Chem. Soc. **123**, 4530 (2001).
[33] T. Demuth, J. Hafner, L. Benco, and H. Toulhoat, J. Phys. Chem. B **104**, 4593 (2000).
[34] L. Benco, T. Bucko, J. Hafner, and H. Toulhoat, J. Phys. Chem. B **108**, 13656 (2004).
[35] L. Benco, T. Bucko, J. Hafner, and H. Toulhoat, J. Phys. Chem. B **109**, 20361 (2005).
[36] I. J. Pickering, P. J. Maddox, J. M. Thomas, and A. K. Cheetham, J. Catal. **119**, 261 (1989).
[37] G. Kresse and J. Hafner, J. Phys. Chem. B **48**, 13115 (1993).
[38] G. Kresse and J. Hafner, J. Phys. Chem. B **49**, 14251 (1994).
[39] G. Kresse and J. Furthmüller, Comput. Mater. Sci. **6**, 15 (1996).
[40] G. Kresse and J. Furthmüller, Phys. Rev. B **54**, 11169 (1996).
[41] J. P. Perdew and A. Zunger, Phys. Rev. B **23**, 5048 (1981).
[42] J. P. Perdew, A. Chevary, S. H. Vosko, K. A. Jackson, M. R. Pedersen, D. J. Singh, and C. Fiolhais, Phys. Rev. B **46**, 6671 (1992); J. P. Perdew and Y. Wang, *ibid.* **33**, 8800 (1986).
[43] J. Paier, R. Hirschl, M. Marsman and G. Kresse, J. Chem. Phys. **122**, 234102 (2005) and references cited therein.
[44] J. Paier, M. Marsman, K. Hummer, I. D. Gerber, and J. G. Angyan, J. Chem. Phys. **124**, 154709 (2006).
[45] J. Paier, M. Marsman, and G. Kresse, J. Chem. Phys. **127**, 024103 (2007).
[46] M. Marsman, J. Paier, A. Stroppa, and G. Kresse, J. Phys.: Condens. Matter **20**, 064201 (2008).
[47] M. Zhou and L. Andrews, J. Phys. Chem. A **104**, 3915 (2000).

[48] E. Uzunova, F. Göltl, G. Kresse, and J. Hafner, J. Phys. Chem. **113**, 5274 (2009).
[49] P. E. Blöchl, Phys. Rev. B **50**, 17953 (1994).
[50] G. Kresse and J. Joubert, Phys. Rev. B **59**, 1758 (1999).
[51] L. Benco, T. Bucko, R. Grybos, J. Hafner, Z. Sobalik, J. Dedecek, and J. Hrusak, J. Phys. Chem. C **111**, 586 (2007).
[52] L. Benco, T. Bucko, R. Grybos, J. Hafner, Z. Sobalik, J. Dedecek, S. Sklenak, and J. Hrusak, J. Phys. Chem. C **111**, 9393 (2007).
[53] G. Kresse, J. Furthmüller, and J. Hafner, Europhys. Lett. **32**, 729 (1995).
[54] A. D. McLean and G. S. Chandler, J. Chem. Phys. **72**, 5639 (1980); R. Krishnan, J. S. Binkley, R. Seeger, and J. A. Pople, *ibid.* **72**, 650 (1980); P. J. Hay, *ibid.* **66**, 4377 (1977); K. Raghavachari and G. W. Trucks, *ibid.* **91**, 1062 (1989).
[55] M. J. Frisch, G. W. Trucks, H. B. Schlegel *et al.*, GAUSSIAN 03, Rev.D01, references cited in www.gaussian.com.
[56] K. P. Huber and G. Herzberg, *Molecular Spectra and Molecular Structure IV, Constants of Diatomic Molecules* (Van Nostrand, New York, 1979).
[57] J. Laane and J. R. Ohlsen, Prog. Inorg. Chem. **27**, 465 (1980).
[58] L. Krim and M. E. Alikhani, Chem. Phys. **237**, 265 (1998).
[59] A. Penkova, K. Hadjiivanov, M. Mihaylov, M. Daturi, J. Saussey, and J.-C. Lavalley, Langmuir **20**, 5425 (2004).
[60] G. J. Moody and J. R. Thomas, *Dipole Moments in Inorganic Chemistry* (Edward Arnold, New York, 1971).
[61] *Handbook of Chemistry and Physics*, 84th ed., edited by D. R. Lide (CRC, Boca Raton, FL, 2003).
[62] T. Grey, J. Gale, D. Nicholson, and B. Peterson, Microporous Mesoporous Mater. **31**, 45 (1999).
[63] W. J. Mortier, *Compilation of Extra-Framework Sites in Zeolites* (Butterworths, London, 1982).
[64] R. Grybos, J. Hafner, L. Benco, and H. Toulhoat, J. Phys. Chem. C **111**, 6454 (2007).
[65] W. Löwenstein, Am. Mineral. **39**, 92 (1954).
[66] T. Takaishi, M. Kato, and K. Itabashi, Zeolites **15**, 21 (1995).
[67] M. Kato, K. Itabashi, A. Matsumoto, and K. Tsutsumi, J. Phys. Chem. B **107**, 1788 (2003).
[68] S. Tavernier and R. Schoonheydt, Zeolites **11**, 155 (1991).
[69] K. Nakamoto, *Infrared and Raman Spectra of Inorganic and Coordination Compounds* (Wiley, New York, 1986).
[70] H. Raebiger, S. Lany, and A. Zunger, Nature (London) **453**, 763 (2008).
[71] R. Ramprasad, W. F. Schneider, K. C. Hass, and J. B. Adams, J. Phys. Chem. B **101**, 1940 (1997).